INTERACTION OF THE X-RAY SOURCE RADIATION WITH THE ATMOSPHERE OF THE NORMAL STAR IN CLOSE BINARY SYSTEMS

M. M. BASKO and R. A. SUNYAEV
Institute of Applied Mathematics, U.S.S.R. Academy of Sciences Moscow, U.S.S.R.

(Received 15 March, 1973)

Abstract. The structure of the stellar atmosphere irradiated by an X-ray source is calculated. On the basis of these numerical calculations an approximate theory of the X-ray reprocessing is formulated. The interaction of X-rays with the stellar atmosphere induces a considerable stellar wind. However, the main part of the X-ray energy is reemitted.

The optical appearances of the close binary system including an X-ray source are discussed. The light curve of such a system is obtained. The mass-loss rate of a star with the size close to that of its Roche lobe is evaluated in the isothermal approximation. Most likely, the accretion of matter on to a neutron star, or a black hole, is the cause of the X-ray luminosity. The accreting matter is supplied with the mass outflow from the normal component induced by X-rays. The X-ray luminosity is shown to have an upper limit stipulated by the outflow saturation.

The model of HZ Her = Her X1 system is constructed which accounts for the observed light curve. The optical appearances of the system are due to the X-ray heating of the face of the X-ray source area of the normal star. The radiation of this hot area is partly reflected by the surface of the disc around the X-ray source. The thin disc is formed by the accretion of matter by the X-ray source. The effective reflection of hard X-rays ($h\nu \sim 15$–30 keV) by the stellar surface is considered. This phenomenon makes it possible to detect those X-ray pulsars whose beam does not intercept the Earth.

The model of Sco X1 as a black hole in a close binary system is discussed.

1. Introduction

Many observed galactic X-ray sources occur in binary systems, one of the components of which being the normal star, and the compact object – X-ray source – the other [1], [2]. The problem of the X-ray re-processing by the atmosphere of the normal star [3], [3a] and connected with it extra mass outflow [4] had arisen long ago, but no adequate theoretical model of this phenomena has been obtained up to now. However, their significance has been confirmed by recent observations of the close binary including the X-ray source Her X1 and the variable star HZ Her [5]-[8]. These observations have shown the X-ray source to be responsible for the HZ Her variability: its side facing the X-ray source is three times brighter than the opposite one [9]–[12]. The energy flux F_{x0} (X-rays) incidence onto the stellar surface greatly exceeds its own energy flux F_0 going out from the centre of the star. In the stellar atmosphere this X-ray flux is transformed into the optical radiation. The temperature of the area of the star facing the X-ray source increases $T_1/T_0 \approx (1 + F_{x0}/F_0)^{1/4}$ and, therefore, its spectral type changes. The rotation of the system results in a periodical variation of the brightness and spectral type of the star with the period being equal to that of the rotation. The approximate theory of X-ray transformation developed in this paper and numerical

Astrophysics and Space Science **23** (1973) 117–158.

calculations are in a good agreement with the observational data*. The principal possibility opening up in this connection is to search for the X-ray sources by methods of the optical astronomy. Theory and observations give the following tests:

(1) The period and phase of the light variation should coincide with those derived form the spectral line analysis.

(2) The brightness variation should be accompanied with the colour and spectral class variation.

(3) At minimum light the star should be of a late enough spectral type. In this case the luminosity proper of the star is low, and the X-ray flux may essentially influence the brightness of the star.

The search for objects of HZ Her variability type [14] among the catalogued variable stars [15] was unsuccessful, and no wonder; for the X-ray sources are not numerous and HZ Her system is obviously peculiar. Its angle i of inclination is close to 90°. For smaller i the amplitude of the light variation and variation in colour diminish. The absorption and emission lines corresponding to different spectral types may be observed in the spectrum of the star.

The anomalously hard X-ray spectrum ($kT_x \sim 20$–30 keV) is another feature of HZ Her system [5, [16]. Because of the high photon energy X-rays penetrate deeply into the atmosphere of the normal star (about the reflection of X-rays by stellar surface see Section 6.1.). The optical depth of these layers (for optical quanta) is large, so the outgoing radiation has a black-body spectrum, and absorption lines corresponding to an early spectral type may appear. A small part of the flux energy is spent on the evaporation of matter from the surface of the star-formation of the induced stellar wind. In the case of HZ Her, the calculations show this stellar wind to exceed $10^{-8}\ \mathcal{M}_\odot\ \mathrm{y}^{-1}$. The accretion of even a small part (1–10%) of this mass flux onto a neutron star can supply a necessary energy for X-ray source Her X1.

A quite different situation might arise for the more soft X-ray spectrum corresponding to $kT_x \sim 1$–5 keV (cf. 4). In this case, the main part of the X-ray flux is absorbed by the outflowing gas and in the region of small optical depth for continuous optical radiation. As a result, the incident energy flux will be re-radiated in ultraviolet and optical lines of helium and highly ionized heavy elements. Only a small portion of absorbed energy will be radiated in the optical range giving rise to a negligible increase of the brightness and to a small change of the spectral type. The main effect in this case is the appearance of the emission lines (in particular, corresponding under usual conditions to the high-temperature plasma) and of a considerable emission below the Balmer discontinuity. In this case for small sin i the system may appear as a normal star with a hot spot which radiates mainly in emission lines. The absorption lines correspond to a low-temperature area (not irradiated by X-rays).

In a close binary system the X-ray flux of different intensity falls on to different

* The results obtained for the classical reflection effect in binary systems [13] cannot be directly employed for the problem considered, because of the specific character of the plasma heating by X-rays.

parts of stellar surface. This results in a greater limb darkening than in the case of a normal star (cf. Section 5.3.1.). The theoretical light curves for a particular model of HZ Her = Her X1 system (cf. Section 6.1.1.) with different $\sin i$ are shown in Figure 1.

The intensity of emission lines varies considerably with the variation in the phase of observation (they should be the most contrast in the phases 0.25 and 0.75), and the latest spectral observations of HZ Her [17], [18] confirm this conclusion. The optical pulsations of HZ Her with period 1.24 s – a response to the pulsating X-ray radiation of Her X1 – should also be displayed best of all in these phases.

In the present paper, the results of numerical calculations for some particular models of the stars (of Main Sequence and giants) irradiated by X-rays are presented (Sections 2.1.–2.3.). The computations furnish the effective surface temperature of the area heated by the X-ray flux; the part of the X-ray flux energy reradiated in optically thin layers of the stellar atmosphere; and the rate of mass loss connected with the influence of intense X-ray flux.

These numerical calculations stimulated the creation of an approximate theory of X-ray transformation by the atmosphere of the normal star. The structure of optically thin (for the optical radiation) and reconstruction of optically thick layers of the star (Section 3.1.) are considered; the cause of temperature and density jump in the outer atmosphere (thermal instability) is analysed (Section 3.3., cf. Figure 3). The simple expressions for the mass outflow from the stellar surface heated by X-rays are given (Section 3.5.). The significant influence of the soft X-rays on the mass flow rate is pointed out (Section 3.6.).

Specific effects connected with the presence of the close and compact companion in a binary system are discussed in the third part of the paper. The rate of mass loss by the star filling or nearly filling its critical Roche lobe is evaluated in isothermal approximation (Section 5.2.). The heating by X-rays significantly affects the mass loss rate in this case too; it increases the velocity of the gas flow at the inner Lagrangian point, and by increasing the gas pressure it broadens the effective cross-section of the flow (Section 5.2.2.). The optical effects (the continuum radiation, the formation of absorption and emission lines etc.) are analysed (Section 5.3.).

In close binary systems including a black hole, a neutron star, or a white dwarf, a considerable part of matter outflowing from the normal component can be captured by the gravitational field of the compact counterpart [19]. The accretion of this matter (most likely the disc accretion [20]–[23], [4]) supplies the energy for the X-ray source. In this case a positive feedback is possible: an extra mass outflow gives rise to the increase of the X-ray luminosity which leads to a further growth of the outflow [4], [24]. The absorption of X-rays in the outflowing gas decreases the feedback coefficient and stabilizes the X-ray luminosity at the level which depends on the parameters of the system, gravitational potential of the compact companion and X-ray spectrum (Section 5.1.). This level may be considerably less than the well-known Eddington limit $L_c = 10^{38}(\mathcal{M}/\mathcal{M}_\odot)$ erg s^{-1}, at which the gravitational attraction of accreting matter is balanced by the light pressure. Possibly, the low (in comparison with the Eddington limit) luminosity of a large number of X-ray sources being the components of

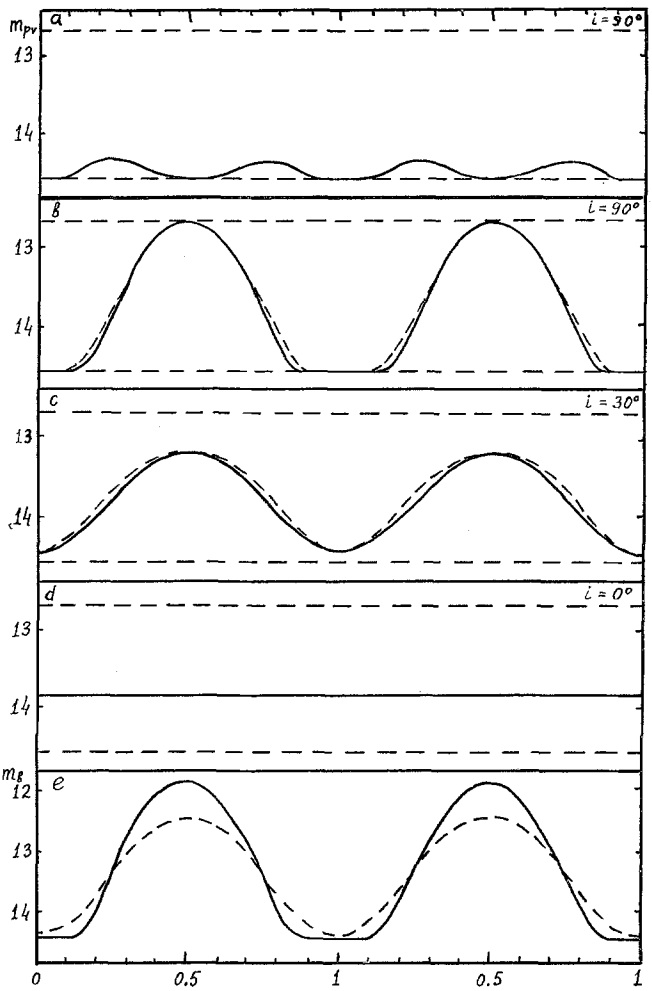

Fig. 1. The theoretical photovisual light curve of HZ Her: 1a – there is no X-ray heating of the atmosphere, the variability is due to the ellipsoidal form of the visible star filling its Roche lobe; 1b, 1c and 1d – the variability due to the X-ray remission in the atmosphere of the normal star is presented for different inclination angles i; the horizontal dashed lines correspond to the minimum and maximum for $i = 90°$; in Figure 1b the solid curve corresponds to the spherical star and the dashed one – to the ellipsoid approximating Roche lobe; in Figure 1c for comparison a sinusoid is plotted as a dashed line; in Figure 1e the bolometric light curves are plotted for $i = 90°$ and $i = 30°$.

close binary systems is accounted for by this mechanism of autoregulation.

The fourth part of this paper deals with the particular models of the systems HZ Her and Sco X1. It is shown that the optical variability of HZ Her with a period of $1^d.7$ can be explained by the action of the X-ray radiation of Her X1 on the visible star. The detailed model of the system is obtained , and its distance and the luminosity of the X-ray source are evaluated. The theoretical light curve in Figure 1b does not agree with the observational data (Figure 2a); it has a sharper maximum than is observed.

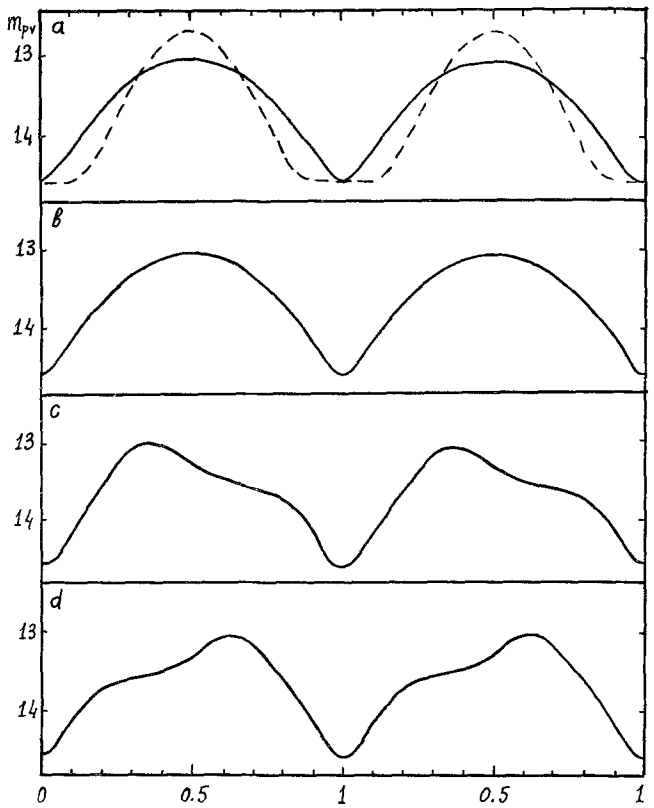

Fig. 2. The theoretical light curve of HZ Her system with the disc eclipses being taken into account; 2a – the comparison of the observational data with Figure 1b; 2b – the light curve of the system with the disc radiation and eclipses being taken into account; 2c and 2d – the light curves with the asymmetric with respect to Lagrangian point hot spot on the stellar surface.

A comparison of the theoretical and experimental light curves suggests that there must exist another optically bright object in the system (cf. also [17]). The disc formed by the matter accreting on the neutron star can be just such an object. The optical luminosity proper of the disc, connected with the gravitational energy liberation in it, is rather small ($\lesssim 10^{33}$ erg s^{-1}) [4]. The disc will radiate by reflecting and transforming the incident ultraviolet and optical radiation of the hot spot on the visible star.* If the radius of the disc is comparable with that of Roche lobe of the X-ray source and the inclination angle $i \approx 70°$–$80°$, then the reflection effect in this system completely accounts not only for the averaged light curve, but also for the more subtle effects found by Kurochkin [25]. The theoretical light curves with occultations of the disc with the star and the star with the disc taken into account are presented in Figures 2b–2d.

The source Her X1 has anomalously hard X-ray spectrum ($kT_x \sim 20$–30 keV). The

* However, the main contribution to the optical luminosity of the disc is due to the transformation of a small part of the X-ray flux irradiating the surface of the disc. Recall that the thickness of the disc increases towards its outer boundary [4].

Compton scattering cross-section exceeds one of the photoionization for the photons with $h\nu > 10$ keV. Hence, a considerable amount of high energy photons incident on the stellar surface will be reflected. As a result, the hard X-rays can be observed on the Earth during those 24 days of 36 when the narrow beam of the soft ($h\nu < 10$ keV) X-rays does not illuminate it. This effect – the reflection of hard X-rays by the surface of the normal component – makes it possible to search for the X-ray pulsars the beam of which does not intercept the Earth. In this case, only hard X-rays can be observed, the soft part of the X-ray spectrum ($h\nu < 10$ keV) being cut off (cf. Section 6.2.3.). The values of albedo and spectral characteristics of the reflected X-ray flux are calculated in [25a].

In Section 6.2. it is noted that the accretion of matter on to a black hole may account for the X-ray luminosity of Sco X1. The optical radiation of this source may originate in the disc of accreting matter (the spectral shape of the disc radiation is identical to that of the observed in Sco X1 [22], [26], [4]) and in the optically thin gas outflow from the normal star. The accreting matter flows out of the normal component – the dwarf or subgiant filling its Roche lobe. The optical luminosity proper of this star is small compared to the optical luminosity of the disc.

The observational effects connected with the rotation of the system (occultations, spectral variability, etc.) are absent because of the negligible inclination angle ($\sin i \ll 1$).

A similar analysis can be performed for a number of other X-ray sources, both identified with the binary systems, or considered up to now to be single. Unfortunately, in the most interesting case of Cyg X1 = BD +34° 3815 system the phenomena under discussion are negligible, since the enormous luminosity of the visible star – the supergiant B0 1b – greatly (30–60 times) exceeds the X-ray luminosity of Cyg X1. Due to small inclination angle ($i \approx 30°$ [10]) the disc around the compact component (black hole?)* formed by accreting matter and reflecting the optical radiation of the normal star does not strongly influence the light curve of this system.

2. Formulation of the Problem and Numerical Calculations

2.1. Basic equations

The computations were performed for the following problem. A spherically-symmetrical time-independent X-ray flux falls onto the surface of the star. Far from the surface it has the spectrum of the form

$$\mathscr{F}_{x0}(\nu) = F_{x0}(h/kT_x) \exp(-h\nu/kT_x) \tag{1}$$

where $F_{x0} = \int_0^\infty \mathscr{F}_{x0}(\nu) d\nu$. Later we shall see that this radiation flux is effectively absorbed in the layer with a thickness small compared with the stellar radius R, and for this reason the dilution of X-rays is neglected. The absorption of X-rays in the atmosphere gives rise to a steady-state spherically-symmetric hydrodynamical flow which obeyes the laws of mass, impulse and energy conservation [27]

* In the note added in proof of [10], the authors noted that the determination of the angle $i \approx 30°$ from the photometric observations [10] and the mass function value allow to obtain $\mathscr{M}_x > 5.6\mathscr{M}_\odot$. The data concerning He II λ 4686 line are not used.

$$\begin{aligned} &\varrho v r^2 = J = \text{const}, \\ &v\frac{\mathrm{d}v}{\mathrm{d}r} + \frac{1}{\varrho}\frac{\mathrm{d}p}{\mathrm{d}r} + \frac{G\mathscr{M}}{r^2} = 0, \\ &v\frac{\mathrm{d}\varepsilon}{\mathrm{d}r} + \frac{p}{\varrho}\frac{1}{r^2}\frac{\mathrm{d}}{\mathrm{d}r}(vr^2) = q^+(T, \varrho, r) - q^-(T, \varrho), \end{aligned} \tag{2}$$

where ϱ is the density, p is the pressure, v is the velocity, ε is the thermal energy per unit mass, q^+ and q^- are the energy production and loss rates per unit mass of the gas, r is the distance from the centre of the star, $\mathscr{M}$ is the mass of the star. In the pressure and thermal energy the electrons, helium and hydrogen ions are taken into account; the ionization energy and the radiation pressure are neglected.

The plasma heating results from the absorption of X-rays due to photoionization of He I, He II and K – shell photoionization of the most abundant heavy elements and their ions (O, C, Ne, N and so on). In this case the equation of X-ray radiation transfer is

$$\frac{\partial \mathscr{F}_x(v, r)}{\partial r} = \frac{x_{\mathrm{H}}\varrho}{m_p}\left[\sum_i c_i(r)\,\sigma_i(v)\right]\mathscr{F}_x(v, r), \tag{3}$$

where x_{H} is the number of hydrogen nuclei per nucleon, m_p is the proton mass,

$$c_i(r) = N(z, Z, r)/\textstyle\sum_z N(z, Z, r)$$

is the fractional abundance of ionization stage z for element Z and $\sigma_i(v)$ is the photoionization cross section of such an ion. The cross-section approximations of this and other atomic processes involved and the method of ionization equilibrium evaluation are given in the Appendix.

Supposing all the absorbed X-ray energy to be converted into a heat, we readily obtain the energy production rate

$$q^+(T, \varrho, r) = \frac{x_{\mathrm{H}}}{m_p}\int_0^\infty \mathscr{F}_x(v, r)\left[\sum_i c_i(r)\,\sigma_i(v)\right]\mathrm{d}v. \tag{4}$$

A comparatively cold and dense plasma near the photosphere has a considerable optical thickness for the spectral range in which plasma mainly radiates, so that the conditions there are close to those of thermodynamical equilibrium. Thus, for the hydrogen ionization equilibrium the Saha's formula was used.

In calculations of the energy loss rate $q^-(T, \varrho)$ three processes were taken into account: the bremsstrahlung q^-_{ff}, the radiative recombinations to the second and higher hydrogen atom levels q^-_r, and recombination losses on the negative hydrogen ions q^-_{H}

$$q^-(T, \varrho) = q^-_{ff}(T, \varrho) + q^-_r(T, \varrho) + q^-_{\mathrm{H}}(T, \varrho). \tag{5}$$

The black-body radiation with the temperature T_{eff} emitted by the photosphere partly compensates the energy losses

$$q^-(T, \varrho) = \frac{4\pi}{\varrho}\int_0^\infty \varkappa(v, T, \varrho)\left[B(v, T) - aB(v, T_{\mathrm{eff}})\right]\mathrm{d}v, \tag{6}$$

where $\varkappa(\nu, T, \varrho)$ is the radiative absorption coefficient,

$$B(\nu, T)=(2h/c^2)\nu^3/[\exp(h\nu/kT)-1]$$

is the black-body radiation intensity. The factor $a\sim 0.5$–1 in (6) arises because of the anisotropy of the outgoing radiation. The term with $B(\nu, T_{\text{eff}})$ in (6) significantly affects the energy loss rate immediately near the photosphere. The calculations performed for $a=1$ and $a=\frac{2}{3}$ show the main results to be practically independent of the particular value of a.

The radiative loss rate of the low-density and high-temperature ($T\sim 10^4$–10^6 K) plasma is considerably affected by the line emission. To treat the problem accurately, when the photoionization dominates other ionization processes (and thus lessens line emission) one should consider many different atomic processes. The accurate solution of the radiative transfer (in continuum and discrete lines) equations is also necessary. Instead, we treat the problem approximately: for the optically thin region the simplified equations are numerically solved, the structure of the optically thick layers being analysed separately (Section 3.1.).

The thermal conductivity, which is of significance in the solar wind formation, was also neglected. For almost all models computed, its contribution to the heating rate even in the hightemperature region is small compared with that of the X-ray absorption.

2.2. Boundary conditions

To solve the system (2) and calculate the outflowing atmosphere, one needs to know the density $\varrho(R)$, the temperature $T(R)$ and the mass flux $J=\varrho v r^2$ at the stellar surface. The mass flux is determined from the equations which must be satisfied at the critical point r_c where the flow velocity equals to the local sound velocity [27]: namely,

$$\begin{aligned} v^2(r_c) &= \frac{5}{3}\frac{\mathscr{R}T(r_c)}{\mu} \\ \frac{G\mathscr{M}}{r_c} &+ \frac{2}{3}\frac{r_c}{v(r_c)}[q^+(r_c)-q^-(r_c)] = \frac{10}{3}\frac{\mathscr{R}T(r_c)}{\mu}, \end{aligned} \tag{7}$$

Where $\mathscr{R}=k/m_p$ is the gas constant, and $1/\mu$ is the particle number per nucleon. Equations (7) are obtained from the system of differential Equations (2), the critical point being singular. The physical meaning of (7) is clarified by the other form of the second equation

$$\frac{v_p^2}{v_s^2}=4-\frac{4\mu}{5}\frac{r_c}{v_s}\frac{q^+(r_c)-q^-(r_c)}{\mathscr{R}T(r_c)}. \tag{8}$$

At the critical point the velocity of sound $v_s=\sqrt{(\frac{5}{3}(\mathscr{R}T(r_c))/\mu)}$ approximates the parabolic one $v_p=\sqrt{(2G\mathscr{M}/r_c)}$. The location of this point depends also on the ratio of the hydrodynamical time-scale $t_{\text{H}}(r_c)\sim r_c/v_s$ to the characteristic thermal time-scale $t_q(r_c)\sim \mathscr{R}T/(q^+-q^-)$.

To obtain the other two boundary conditions, one needs to know the optical depth of the atmosphere for different frequencies

$$\tau(\nu, r) = \int_r^\infty \varkappa[\nu, T(r), \varrho(r)]\,\mathrm{d}r. \tag{9}$$

The radiative absorption coefficient $k(\nu, T, \varrho)$ was calculated for the same processes as were taken into account in the energy loss rate, i.e. for free-free absorption, photoionization of the second and higher hydrogen atom levels and photoabsorption on the negative hydrogen ions. The expression (9) was averaged with the Planckian distribution as a weight function

$$\bar{\tau}(r) = \int_0^\infty \tau(\nu, r)\, B(\nu, T_{\mathrm{eff}})\,\mathrm{d}\nu \Big/ \int_0^\infty B(\nu, T_{\mathrm{eff}})\,\mathrm{d}\nu. \tag{10}$$

The layer with an averaged optical depth equal to $\frac{2}{3}$ was adopted to be the lower boundary of the atmosphere. At so defined a boundary between the atmosphere and the photosphere, the following relationship must be satisfied,

$$\tfrac{3}{2}\pi \int_0^\infty \tau(\nu, R)\, B(\nu, T_{\mathrm{eff}})\,\mathrm{d}\nu = bT_{\mathrm{eff}}^4, \tag{11}$$

where b is the Stephan-Boltzmann constant. We assume that the plasma temperature in this layer is T_{eff} and the black-body radiation with the intensity $B(\nu, T_{\mathrm{eff}})$ goes out of it.

A considerable part of hard X-rays may penetrate within this boundary and, its energy being converted into the heat, increase the emergent radiative energy flux. This allows to obtain the other condition for the boundary between the atmosphere and the photosphere in the form

$$bT_{\mathrm{eff}}^4 = bT_0^4 + \int_0^\infty \mathscr{F}_x(\nu, R)\,\mathrm{d}\nu \tag{12}$$

where T_0 is the effective stellar temperature when the X-ray flux is absent. Thus, the density $\varrho(R)$ and the temperature $T(R) = T_{\mathrm{eff}}$ at the lower boundary of the atmosphere are determined from Equations (11) and (12) ($\tau(\nu, R)$ in (11) is a function of the density).

2.3. The results of numerical calculations

The results of numerical calculations for a number of stellar models (S – the Main Sequence star, G – the giant G0, HZ and HZS – the star with parameters close to those of discussed HZ Her models [10], [12], [17] see also Section 6.1.1.) are presented below. After the letters marking the stellar model type $\beta = F_{x0}/bT_0^4$ is given in parentheses. For all models except HZS (20) the X-ray spectrum was assumed to be cut off at $h\nu < 1$ keV. In HZS (20) model the spectral interval $h\nu < 1$ keV contained 5% of the total energy flux.

The parameters and main results for the models calculated are listed in Table I, where $\eta = \varrho_c v_c^3 r_c^2 / 2R^2 F_{x0}$ is the part of the primary X-ray energy flux converted into

the kinetic energy of the gas flow, τ_x is the optical depth of the boundary between the atmosphere and the photosphere for the photoabsorption of photons with the energy $h\nu = 1$ keV, τ_{opt} is the optical depth (for the optical radiation) of the layer where the major part ($h\nu \sim kT_x$) of X-rays is absorbed. It was evaluated according to the solution for the optically thick region given below (Section 3.1.).

In Figures 3 and 4 the distributions of the temperature, the pressure, the Mach number and the fractional abundances of O VIII (c_O) and He II (c_{He}) in the upper atmosphere for the model S(10) are shown. For the models S(1), G(10) and HZ(20) the curves qualitatively are the same. The atmosphere parameters for these models at points *a*, *b* and *c* are listed in Table II. In Figures 5 and 6 the same quantities as in Figures 3 and 4 are plotted for the model HZS(20).

3. The Approximate Description of the Outflowing Atmosphere

3.1. Reconstruction of the lower atmosphere

The analysis of the structure of the optically thick for the optical radiation ($\bar{\tau} \gg 1$) layers performed below justifies to some extent the obtained above boundary conditions and enables one to imagine how the region under the photosphere undergoing the X-ray action is reconstructed.

In the lower atmosphere ($\bar{\tau} \gg 1$) the equations of hydrostatics and radiative heat transfer are valid. For the plane-parallel atmosphere they are

$$\frac{dp}{dr} = -\varrho \frac{G\mathcal{M}}{R^2}, \qquad F_0 + F_x(r) = -\frac{16b}{3} \frac{T^3(r)}{\bar{\kappa}(T, \varrho)} \frac{dT}{dr}, \tag{13}$$

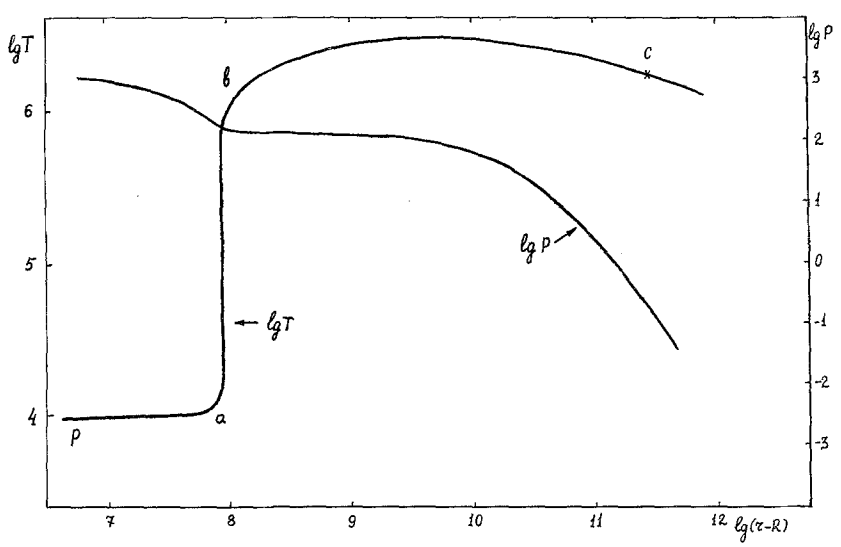

Fig. 3. The temperature and density distribution over the stellar atmosphere in the model S (10).

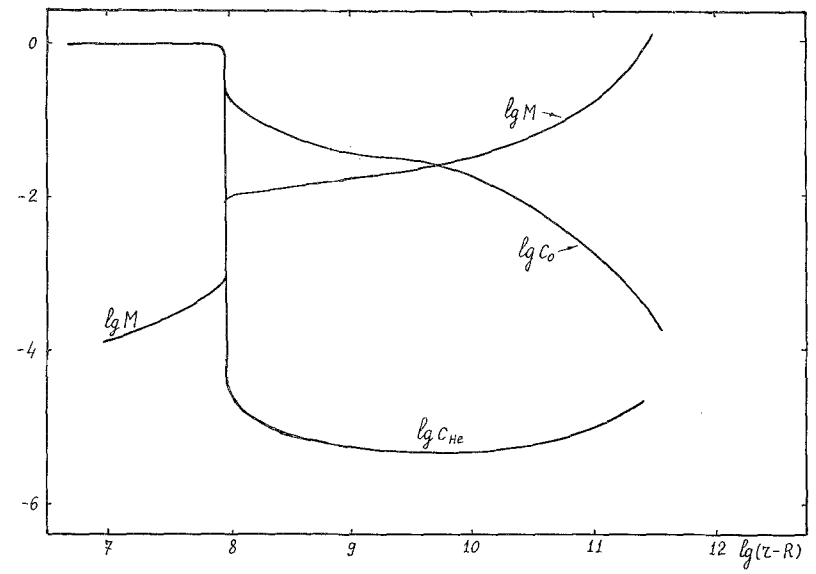

Fig. 4. The distribution of the Mach number M and the fractional abundances of O VIII (C_O) and He II (C_{He}) over the stellar atmosphere in the model S (10).

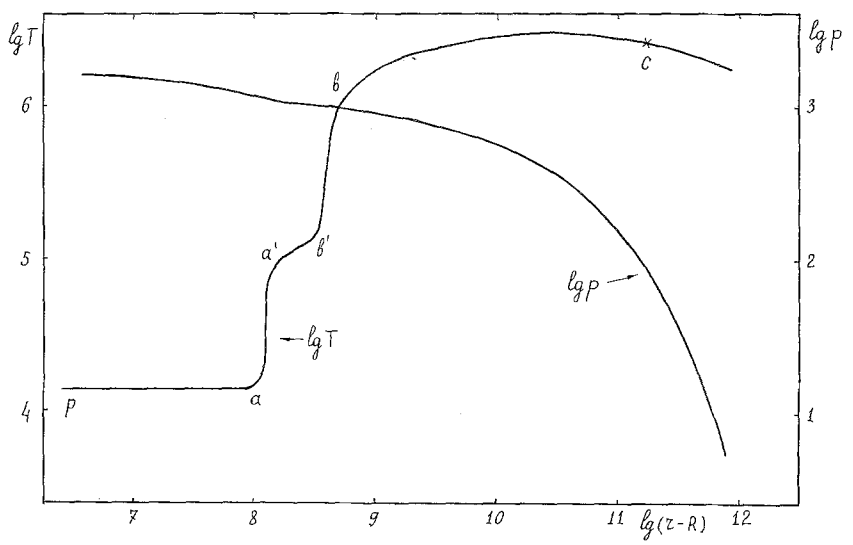

Fig. 5. The temperature and density distribution over the stellar atmosphere in the model HZS (20).

where $\bar{\kappa}(T, \varrho)/\varrho$ is the Rosseland average opacity, $F_0 = bT_0^4$ is the own stellar energy flux, $F_x(r) = \int_0^\infty \mathcal{F}_x(\nu, r)\mathrm{d}\nu$ is the X-ray energy flux. Henceforth in this section we adopt

$$\bar{\kappa}(T, \varrho) = \varrho^2 \varphi(T), \tag{14}$$

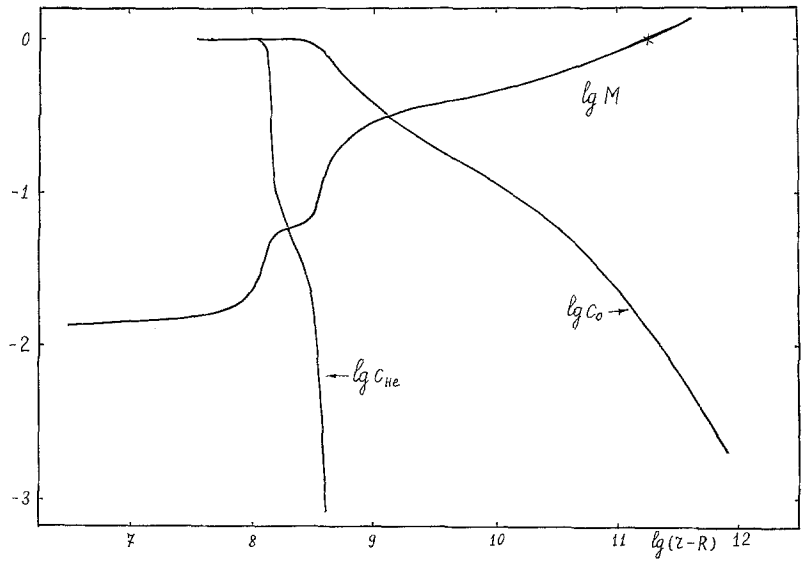

Fig. 6. The distribution of the Mach number and the fractional abundances of O VIII and He II over the stellar atmosphere in the model HZS (20).

and introduce a new variable

$$y = \frac{x_H}{m_p} \int_r^R \varrho(r)\, dr. \tag{15}$$

From Equation (13), (14) and (3) we readily obtain

$$\begin{aligned} p &= \frac{\mathscr{R} T \varrho}{\mu} = \frac{G\mathscr{M}}{R^2} \frac{m_p}{x_H} (y + y_0), \\ F_0 + F_x(y) &= \frac{16b}{3} \frac{x_H}{m_p} \frac{T^3}{\varrho \varphi(T)} \frac{dT}{dy}, \\ F_x(y) &= \int_0^\infty \mathscr{F}_x(v, R) \exp[-\sigma(v)\, y]\, dv. \end{aligned} \tag{16}$$

The third equation in (16) is the solution of Equation (3) for the low-temperature plasma, when heavy elements are low ionized and $\sum_i c_i(r)\sigma_i(v) = \sigma(v)$. From conditions at the upper photosphere boundary we have $y_0 = (x_H/m_p)[\mathscr{R} T_{eff} \varrho(R)/\mu]/(G\mathscr{M}/R^2)$. The solution of the system (16) can be written in terms of quadratures as

$$(y^2/2 + y y_0) F_0 + \int_0^y (\xi + y_0) F_x(\xi)\, d\xi = \left(\frac{x_H}{m_p}\right)^2 \frac{16b}{3} \frac{R^2}{G\mathscr{M}} \frac{\mathscr{R}}{\mu} \int_{T_{eff}}^T \frac{\xi^4 d\xi}{\varphi(\xi)}. \tag{17}$$

TABLE I

	$\frac{\mathcal{M}}{\mathcal{M}_\odot}$	$\frac{R}{R_\odot}$	T_0	T_{eff}	$\varrho(R)/m_p$ (cm^{-3})	J ($\mathcal{M}_\odot$/yr. ster)	η	$\frac{kT_x}{\text{(keV)}}$	τ_x	τ_{opt}
$S(10)$	1	1	5700°	9500°	1×10^{15}	1.2×10^{-11}	2.4×10^{-6}	5	4.6	30
$S(1)$	1	1	5700°	5800°	1.8×10^{17}	3.5×10^{-14}	10^{-10}	5	3×10^2	300
$G(10)$	2.5	6.3	5400°	8500°	2.8×10^{14}	1.2×10^{-8}	1.2×10^{-3}	5	15.5	4
HZS(20)	1.7	3	7000°	14400°	5.1×10^{14}	1.2×10^{-8}	6.2×10^{-4}	15	11.3	40
HZ(20)	1.7	3	7000°	14200°	4×10^{14}	6.5×10^{-9}	5×10^{-4}	15	12	40

TABLE II

		$r-R$ (cm)	$T(r)$	$\varrho(r)/m_p$ (cm^{-3})	$M(r)$	$C_{\text{O}}(r)$	$C_{\text{He}}(r)$	$F_x(r)/F_{x0}$
$S(1)$	a	1.8×10^8	9×10^{3}°	6×10^{12}	4×10^{-5}	1	1	1
	b	1.9×10^8	10^{6}°	3.6×10^{10}	6×10^{-4}	0.15	3.4×10^{-5}	1
$G(10)$	a	5.8×10^8	1.2×10^{4}°	7×10^{13}	2.2×10^{-2}	1	1	0.945
	b	6.4×10^8	5.2×10^{5}°	1.4×10^{12}	0.17	0.5	1.2×10^{-4}	0.975
	c	9.4×10^{10}	2.4×10^{6}°	9.1×10^{10}	1	2.5×10^{-2}	6×10^{-6}	0.994
HZ(20)	a	2.7×10^8	1.8×10^{4}°	1.7×10^{14}	2×10^{-2}	1	1	0.95
	b	3.3×10^8	7×10^{5}°	3.6×10^{12}	0.16	0.52	5.5×10^{-5}	0.96
	c	7×10^{10}	2.8×10^{6}°	2×10^{11}	1	2×10^{-2}	5×10^{-6}	0.99

For realistic forms of dependence $\varphi(T)$ on the temperature ($\mathrm{d}\varphi/\mathrm{d}T \leqslant 0$)

$$\int_{T_{\mathrm{eff}}}^{T} \frac{\xi^4 \mathrm{d}\xi}{\varphi(\xi)} \to \infty \quad \text{when} \quad T \to \infty \tag{18}$$

and

$$\left| \int_0^y (\xi + y_0) F_x(\xi) \mathrm{d}\xi \right|$$

is limited when $y \to \infty$; therefore, in deep layers of the star the contribution of the second term in Equation (17) – as might be expected – is negligible. The absorption of X-rays gives rise to a reconstruction close to the stellar surface layers, but for large $y \gg \sigma^{-1}(kT_x/h)$ this reconstruction vanishes, and the stellar structure is described with the solution obtained for the non-irradiated by X-rays star. This conclusion holds for more general forms of $k(T, \varrho)$ than those given by (14) but it is then less obvious.

In the case when the opacity is due to the free-free absorption only, $\varphi(T) = k_0 T^{-7/2}$. Then for the monochromatic with the frequency ν X-ray flux the Equation (17) becomes

$$\frac{32}{51}\left(\frac{x_{\mathrm{H}}}{m_p}\right)^2 \frac{b}{k_0} \frac{R^2}{G\mathcal{M}} \frac{\mathcal{R}}{\mu} [T(y)^{17/2} - T_{\mathrm{eff}}^{17/2}] = (y^2/2 + yy_0) F_0 + \\ + \frac{F_x(R)}{\sigma(\nu)} \{y_0 + \sigma^{-1}(\nu) - [y + y_0 + \sigma^{-1}(\nu)] \exp[-\sigma(\nu) y]\}. \tag{19}$$

The expression (19) for $y \to \infty$, when the X-ray flux may be neglected, reduces to the well-known relationship in the theory of grey atmosphere [28]

$$T^4(\tau) = T_0^4 (\tfrac{3}{4}\tau + 0.71), \tag{20}$$

where $\tau = \int_r^R k_{ff}(r)\mathrm{d}r$ is the optical depth with respect to free-free absorption. From the Table I we can see that X-rays reach the layers with the optical depth up to 100 for $k_{ff} = 2 \times 10^{-24} N_e (\sum_i N_i Z_i^2) T^{-7/2}$ cm^{-1}.

The density distribution may be now easily obtained from the first equation of (16)

$$\varrho(y) = \frac{m_p}{x_{\mathrm{H}}} \frac{G\mathcal{M}}{R^2} \frac{\mu}{\mathcal{R}T(y)} (y + y_0). \tag{21}$$

3.2. Characteristic zones of the upper atmosphere

The typical distributions of the temperature, the pressure, the velocity and the ion abundances are shown in Figures 3 and 4. The whole atmosphere breaks up into three characteristic zones strongly resembling the solar chromosphere, transition layer and corona.

In *pa* zone adjoining the photosphere the density is rather high, the temperature only slightly differs from T_{eff}, the Mach number $M(r) = v(r)/v_s(r) \ll 1$. The X-ray plasma heating is completely balanced with the radiative cooling. The optical depth of this region for quanta with $h\nu \sim kT_{\mathrm{eff}}$ is of the order of unity. The ionization of heavy

elements is low and X-rays are absorbed according to calculations in [29], [30]. The dimensions of this region are $\sim 10^8$ cm.

The region *ab* is a narrow transition layer in which the thermal equilibrium is violated (the heating exceeds the cooling). Consequently, the temperature rapidly increases by one or two orders of magnitude under an almost constant pressure, and the flow velocity grows remaining subsonic. In the matter crossing this layer helium and other heavy elements become highly ionized. The thickness of this layer is of the order 10^6 cm, i.e. is close to the thickness of the similar zone in the solar atmosphere [31].

Above *ab* zone the high-temperature and low-density *bc* region resembling corona is situated. The temperature of the gas in the X-ray radiation field depends on the X-ray spectrum and intensity and on the plasma density 32]. The calculations including adiabatical cooling and Compton scattering [33], [4] give the results differing from those of [32] (where the main processes were the X-ray absorption and the radiative cooling) for the low-density plasma. However, the results of our rough treatment are close to those of [32]. In *bc* region the temperature is nearly constant and close to 10^6 K. The radiative energy losses are compensated by the X-ray energy input (however, not so accurately as in *pa* region) until at low densities the adiabatic cooling becomes too large. With the increasing distance from the stellar surface the degree of ionization of heavy elements increases. The whole region *abc* is optically thin for the frequencies $h\nu \sim kT_{\text{eff}}$. The rapid increasing of the temperature (and the sound velocity) in *ab* zone and decreasing of the parabolic velocity with growing distance from the stellar surface lead to Equation (8) being satisfied in *abc* region. The plasma temperature being constant or growing in *bc* region, the mass flow velocity becomes equal to the sound one (the flow passes through the critical point) when the latter is of the order of the parabolic one.

3.3. Thermal instability and temperature jump

In the narrow (compared to the stellar radius R and the height of the exponential atmosphere $H=(\mathcal{R}T/\mu)/(G\mathcal{M}/R^2))ab$ layer the temperature and density jump takes place. It occurs because of the specific dependence of the adopted energy loss rate on the temperature and density under the fixed pressure: it has a maximum at $T=T_m$ (Figure 7)

$$\frac{\partial}{\partial T} q^{-}(T, \varrho)|_{T=T_m,\, p=\text{const}} = 0. \tag{22}$$

The ratio T_m/T_{eff} weakly depends on T_{eff} and the density and is confined to the interval $1<T_m/T_{\text{eff}}<2$.

The region $T>T_m$ is unstable; for the plasma cannot be in the thermal equilibrium under the fixed pressure and energy production rate. The increase of temperature (and consequently, the decrease of density) are followed with the drop in the cooling rate, which results in further growth of temperature and diminution of density. However, the temperature of plasma heated by X-rays cannot grow infinitely. With the increasing temperature and decreasing density the recombination rate $w \propto \varrho T^{-1/2} \propto T^{-3/2}$

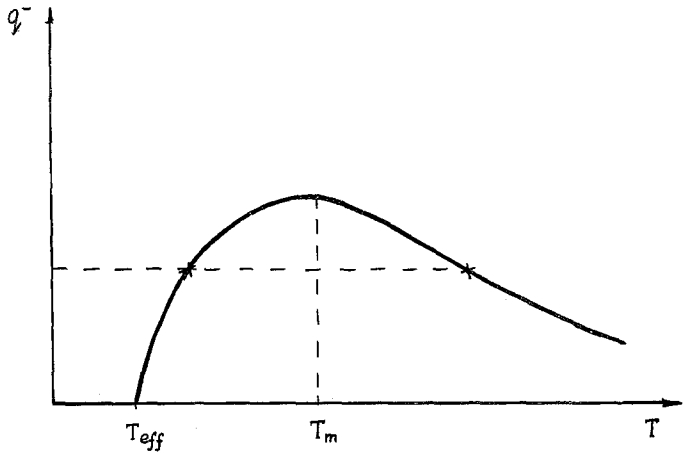

Fig. 7. The dependence of the adopted energy loss rate in plasma under the fixed pressure.

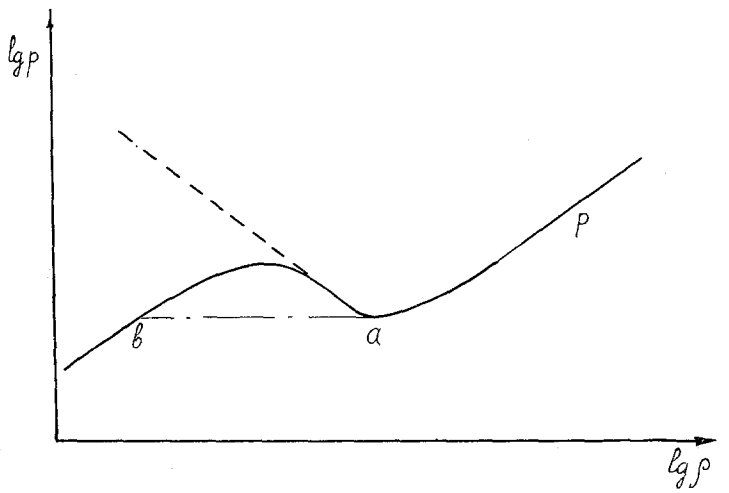

Fig. 8. The dependence $p(\varrho)$ for plasma in the thermal equilibrium under the fixed energy production rate (dashed line) and in the X-ray radiation field of the given intensity (solid curve). At a low enough density the ionization of heavy elements results in the rapid decrease of the heating rate.

rapidly drops, the photoionization rate being independent of them. The growth of the ionization degree of heavy elements and the corresponding drop in heating rate set an upper limit on the temperature $T<T_{\max}$, and result in the establishment of a thermal equilibrium $q^+=q^-$. For this reason, the solid curve in Figure 8 corresponding to the thermal equilibrium of the gas in the X-ray radiation field of the fixed intensity deviates downwards from the dashed one corresponding to the unstable region of the gas in thermal equilibrium under the fixed energy production rate. The limiting temperature $T_{\max}$ is determined by the X-ray spectrum [32], [33].

With the increasing distance from the stellar surface the pressure must diminish,

so that in a static atmosphere the temperature and density jump corresponding to the region *ab* in Figure 8 should be present. In the outflowing atmosphere the thermal equilibrium of the gas passing from *pa* region to the region *bc* is violated, the gas is heated and accelerated. The attenuation of the X-ray flux does not alter this qualitative pattern, for it is negligible in the narrow layer *ab*. The width of *ab* layer may be estimated from

$$r_b - r_a \approx v(r_b)\frac{3}{2}\frac{\mathscr{R}(T_b - T_a)}{\mu q^+(T_b, \varrho_b, r_b)}. \tag{23}$$

The actual jump will have much more complicated structure, the real dependence of the cooling and heating rates on the plasma temperature, density and the X-ray spectrum for the gas with normal chemical abundancies being taken into account. Then the presence of intermediate zones with plasma being in the thermal equilibrium and $T<T_{\max}$ is possible. Such intermediate zone appears, for instance, when the X-ray absorption on helium atoms and ions is taken into account (see Figures 5 and 6). It should be noted that the physical processes in the solar atmosphere stipulate the existence of a layer similar to the described above region *ab* [31]. The analogous thermal instability is discussed in the theory of interstellar gas [34], [35].

3.4. The quasistatic region *pab*

The region *pa* may be described accurately enough with the equations of thermal and hydrostatic equilibrium

$$\begin{aligned} &\frac{\mathrm{d}p}{\mathrm{d}r} = -\varrho\frac{G\mathscr{M}}{R^2}, \\ &q^+(T, \varrho, r) = q^-(T, \varrho), \\ &\frac{\partial \mathscr{F}_x(\nu, r)}{\partial r} = \frac{x_{\mathrm{H}}}{m_p}\varrho\sigma(\nu)\mathscr{F}_x(\nu, r). \end{aligned} \tag{24}$$

It is convenient to calculate the structure of this region from the jump boundary (the point *a*) up to the layer with $\bar{\tau}=\frac{2}{3}$ and $T=T_{\mathrm{eff}}$. The temperature $T_a \approx T_m$ of the point *a* can be obtained from Equation (22). As a boundary conditions the X-ray flux $\mathscr{F}_x(\nu, r_a)$ at the jump and Equation (12) allowing to find T_{eff} are used.

Passing through the jump gas is heated. Over the jump at the point *b* the photoionization of heavy elements results in a decrease of the heating rate and the reestablishment of the thermal equilibrium. If $M(r_b)\ll 1$ then gas passes through the jump practically under the constant pressure. Due to the narrowness of the jump the X-ray attenuation may be neglected. Thus, the jump is described with the following relations

$$p(T_a, \varrho_a) = p(T_b, \varrho_b); \qquad \mathscr{F}_x(\nu, r_a) = \mathscr{F}_x(\nu, r_b); \qquad q^+(r_b) = q^-(r_b). \tag{25}$$

As we can see from Equation (8) the condition $M(r_b)\ll 1$ is fulfilled when $\mathscr{R}T_{\max} \ll G\mathscr{M}/r_b$ ($v_s \ll v_p$). In the opposite case $v_s \gg v_p$ the transition to a supersonic flow takes place in the jump region and the first equation in (25) should be replaced with the

impulse conservation law for gas passing through the jump

$$p(r_a) = p(r_b) + \varrho(r_b)\, v^2(r_b) \tag{26}$$

The expression for $v(r_b)$ is given below. This case may be of interest for the stars with a small gravity acceleration near the surface – for supergiants and stars filling their Roche lobes. The density ϱ_b may be roughly estimated from the conditions that $T_b \approx T_{\max}$ and the X-ray photoionization time for the ion O VIII approximates the recombination time of O IX, i.e. their numbers per unit volume are approximately equal and

$$\varrho_b \approx \frac{m_p}{x_O \alpha_9(T_b)} \int_{\nu_8}^{\infty} \frac{\mathscr{F}_x(\nu, r_b)}{h\nu}\, \sigma_O(\nu)\, d\nu \approx \frac{m_p}{x_O} \frac{F_x(r_b)}{h\nu} \frac{\sigma_O(\nu)}{\alpha_9(T_b)}, \tag{27}$$

where (and hereafter) the last expression is for the monochromatic X-ray flux, and indices '8' and '9' correspond to ions O VIII and O IX. At $r > r_b$ heavy elements (the oxygen in our case) are highly ionized by X-rays $N_8 \ll N_9$

$$c_O \approx \frac{N_8}{N_9} = \frac{x_O \varrho(r)\, \alpha_9(T_b)}{m_p \int_{\nu_8}^{\infty} [\mathscr{F}_x(\nu, r)/h\nu]\, \sigma_O(\nu)\, d\nu} \approx \frac{x_O \varrho(r)}{m_p} \frac{h\nu}{F_x(r)} \frac{\alpha_9(T_b)}{\sigma_O(\nu)}. \tag{28}$$

The X-ray absorption in this region is stipulated by the recombination rate. Indeed, combining Equations (3) and (28) we readily obtain

$$\frac{d}{dr} \int_{\nu_8}^{\infty} \frac{\mathscr{F}_x(\nu, r)}{h\nu}\, d\nu = \alpha_9(T_b)\, x_O \frac{\varrho^2(r)}{m_p^2} \approx \frac{1}{h\nu} \frac{dF_x(r)}{dr}. \tag{29}$$

For the isothermal exponential atmosphere $\varrho(r) = \varrho_b \exp[-(r - r_b)/H]$, where $H = (\mathscr{R} T_b/\mu)/(G\mathscr{M}/R^2)$, and monochromatic X-rays from Equation (29) one finds that

$$F_x(r_b) = F_{x0} - h\nu \alpha_9(T_b) \frac{x_O \varrho_b^2}{m_p^2} \frac{H}{2}. \tag{30}$$

Now from Equations (27) and (30) we obtain the value of the density at the point b

$$\varrho_b \approx \frac{m_p}{\sigma_O(\nu)\, H} \left[\sqrt{1 + 2 \frac{\sigma_O(\nu)}{\alpha_9(T_b)} \frac{F_{x0}}{h\nu} \frac{\sigma_O(\nu)\, H}{x_O}} - 1 \right]. \tag{31}$$

3.5. The approximate description of the mass flow

In the region bc plasma may be treated as isothermal with the temperature $T = T_b \approx T_{\max}$. This enables us to integrate the second equation in (2) and obtain the velocity distribution (the constant of integration is determined from the conditions of transition to the supersonic flow)

$$M^2(r) - \ln[M^2(r)] = 4 \ln[4v_s^2/v_p^2(r)] + v_p^2(r)/v_s^2 - 3, \tag{32}$$

where $v_p^2(r)=2G\mathscr{M}/r$, $v_s=\sqrt{(\mathscr{R}T_b/\mu)}$ is the isothermal speed of sound, $M(r)=v(r)/v_s$. Equation (32) for each value of r admits of two solutions: $M_1(r)<1$ and $M_2(r)>1$ corresponding to subsonic and supersonic flows. The flow is subsonic for $r<G\mathscr{M}\mu/2\mathscr{R}T_b$ and supersonic one for $r>G\mathscr{M}\mu/2\mathscr{R}T_b$. When $M(r_b)\ll 1$ the Equation (32) allows to evaluate the flow velocity at the point b from

$$v(r_b)\approx v_s[v_p^2(R)/2v_s^2]^2\exp[-v_p^2(R)/2v_s^2]=v_s(R/H)^2\exp(-R/H), \tag{33}$$

where H is the height of the isothermal atmosphere.

If one knows the velocity distribution in the region bc, one can easily obtain from the continuity equation the density distribution $\varrho(r)$

$$\varrho(r)\,v(r)\,r^2=\varrho_b v_b r_b^2. \tag{34}$$

Now, when $T(r)=T_b$ and $\varrho(r)$ are known, from (3) we can obtain the X-ray flux $\mathscr{F}_x(\nu, r)$ in the region considered.

Thus, the approximate description allows for a given X-ray flux in the jump completely calculate the outflowing atmosphere. The expression for the mass flux in case $M(r_b)\ll 1$ is

$$J=\varrho v r^2=\varrho_b v_s R^2[v_p^2(R)/2v_s^2]^2\exp[-v_p^2(R)/2v_s^2]. \tag{35}$$

In analogous way for $M(r_b)\gtrsim 1$ from Equation (32) we have

$$J=\varrho_b v_s R^2\{4\ln[4v_s^2/v_p^2(R)]+v_p^2(R)/v_s^2-3\}^{1/2}. \tag{36}$$

The calculations according to the given above Equations (31) and (35) show the mass loss rate for model HZ (20) be 4 times more than the value presented in Table I.

3.6. Influence of the soft part of X-ray spectrum

When the X-ray flux contains a considerable amount of energy in the soft part of its spectrum ($h\nu<1$ keV) light elements (He, C, N) are almost completely ionized in the high-temperature region bc and plasma is transparent for soft X-rays. In pa region at high density and low temperature these elements are low ionized, and due to the large photoabsorption cross section soft X-rays cannot deeply penetrate into this region. They are effectively absorbed in the jump zone. Hence, the soft part of X-ray spectrum may give the main contribution to the plasma heating rate even when it contains only a small portion of the total energy. The increasing of the soft X-ray flux shifts the jump towards the photosphere, increases plasma density in the jump and intensifies the mass flow. In HZS (20) model with the soft part of X-ray spectrum containing only 5% of the total energy flux the mass flux is two times more than in HZ (20) model with the X-ray spectrum cut off at $h\nu<1$ keV.

The presence of soft X-rays results in a more complicated structure and a considerable width of the jump. In this case the approximate description of the outflowing atmosphere is less definite than in the case of hard X-ray spectrum. It should be noted that the stellar mass loss rate is affected by soft X-rays emitted in the high-

temperature region *bc*. About the half of the X-ray flux absorbed in this region is emitted towards the jump.

4. X-Ray Transformation

A negligible part of the X-ray energy flux is transformed into the energy of stellar wind ($\eta < 10^{-2}$, see Table I), the major part being reemitted. The fraction of the X-ray flux penetrating within the atmosphere boundary is one of the most important quantities characterizing the stellar atmosphere. We shall illustrate its dependence on the stellar parameters and the mean energy of X-ray quanta on the simple example of the plane isothermal atmosphere $\varrho = \varrho(R)\exp(-h/H)$ with the opacity due to the free-free absorption only. From the condition $\bar{\tau}_{\text{opt}} = \int_0^\infty \kappa(T_{\text{eff}}, \varrho)\mathrm{d}h = \int_0^\infty \varphi(T_{\text{eff}})\varrho^2 \mathrm{d}h = \varphi(T_{\text{eff}}) \times \varrho^2(R)H/2 = \frac{2}{3}$ we obtain the boundary density $\varrho(R) = \sqrt{[(\frac{4}{3})\varphi^{-1}(T_{\text{eff}})H^{-1}]}$. At the boundary R between the atmosphere and the photosphere the optical depth for X-ray quanta is $\bar{\tau}_x = 1/m_p \int_0^\infty \sigma_x \varrho \mathrm{d}h = \sigma_x \varrho(R)H/m_p = [(4\sigma_x^2 H/3m_p^2)\varphi^{-1}(T_{\text{eff}})]^{1/2}$.

When $\varphi(T_{\text{eff}}) = \kappa_0 T_{\text{eff}}^{-7/2}$, $\sigma_x \propto T_x^{-3}$ and $H = (\mathscr{R}T_{\text{eff}}/\mu)/(G\mathscr{M}/R^2) \propto T_{\text{eff}}/g$ we find that

$$\tau_x = \sqrt{\frac{4\mathscr{R}}{3\mu}} \frac{\sigma_x}{m_p} \frac{1}{\sqrt{g}} T_{\text{eff}}^{1/2} \varphi^{-1/2}(T_{\text{eff}}) \propto T_{\text{eff}}^{2.25} T_x^{-3} g^{-1/2}. \tag{37}$$

When $\tau_x \ll 1$ the major part of the X-ray flux penetrates within the photosphere. For this a sufficiently hard X-ray spectrum is required (high T_x). However, the dependence on T_{eff} and the gravity acceleration g near the stellar surface is also of importance.

(a) *The Case* $\tau_x \ll 1$

The major part of the X-ray flux passes through the photosphere boundary and is converted into the black-body optical radiation. The effective stellar surface temperature becomes approximately $\sqrt[4]{(1 + F_{x0}/F_0)}$ times greater. A small amount of energy is absorbed in *pa* region and its structure does not differ significantly from that of the analogous region of the star with the effective temperature $T_1 = T_0 \sqrt[4]{(1 + F_{x0}/F_0)}$. In the reversing layer $\mathrm{d}T/\mathrm{d}r < 0$, and the absorption lines should be formed. However, for large values of the X-ray flux the situation may arise when the thermal balance in *pa* region is determined not by the energy supplied with the photospheric radiation but by the X-ray heating. In this case the temperature above the photosphere is rising – $\mathrm{d}T/\mathrm{d}r > 0$ – and the emission line formation in *pa* region is possible.

In stellar atmospheres with the low effective temperature $T_{\text{eff}} \sim 4000°$–$7000°$ the main contribution to the opacity is due to photoabsorption by ions H^- which is of low efficiency. The optical spectrum is formed at a depth $y = x_H/m_p \int_0^\infty \varrho \mathrm{d}r$ which is difficult for X-ray quanta to reach. The X-ray heating of the outer layers raises the electron temperature and increases the number of free electrons. Because of the more efficient opacity mechanisms (free-free absorption and absorption on hydrogen atoms) the Planckian spectrum is formed at a smaller depth y, a greater part of the X-ray flux penetrates into the photosphere, and the outgoing flux of the equilibrium optical radiation increases. Thus, the X-ray heating altering the atmosphere structure of the

cold star (shifting the photosphere boundary to low-density layers) increases the part of the energy flux re-radiated in the optical spectrum interval. Just for this reason in S (10) model with $kT_x = 5$ keV about 70% of the X-ray energy flux penetrates within the photosphere, when for S (1) (the heating is inefficient) this part contains only 10% of the total energy flux.

(b) *The Case* $\tau_x \gtrsim 1$

A considerable part of the X-ray flux is absorbed in the optically thin for the optical radiation region. For stars with a high mass loss rate the X-ray absorption in the high-temperature region *bc* may be of importance. The absorbed energy is radiated in ultraviolet and soft X-rays, mainly in emission lines of highly ionized heavy elements and helium. The presence of external X-rays strongly affecting the ionization equilibrium increases the energy flux in continuum and decreases the emission in a number of lines.

Part of the X-ray flux is absorbed in the low-temperature region *pa* between the photosphere and the jump. As was mentioned above, it causes the weakening of the absorption lines and appearance of the strong emission lines and in particular emission Balmer discontinuity.

It is possible for the optical radiation of the hot and optically thin region *pab* to exceed both the own stellar energy flux and the reemitted by the optically thin layers X-ray flux. In this case the spectral distribution of the continuum should considerably differ from that of the black-body radiation.

5. Effects Connected with the Presence of the Second Component

5.1. Self-consistent regime of the mass outflow and accretion in binary systems

If the luminosity of the X-ray source in a binary system is due to the accretion of the gas flowing out from the normal companion, a positive feedback may occur [4], [24]. An extra mass outflow causes the X-ray luminosity to increase, the latter resulting in the further growth of mass flux. It might seem that, for the amplification factor $a > 1$, the X-ray luminosity should increase to the Eddington limit $L_c = 10^{38}(\mathcal{M}/\mathcal{M}_\odot)$ erg s^{-1} We shall show below that another X-ray luminosity limit exists, which is determined by the X-ray spectrum and parameters of the binary system.

For the low intensity of the X-ray flux the mass outflow rate is directly proportional to it. The increase of the X-ray flux shifts the jump to a more dense layer, and the mass outflow rate grows. The X-ray absorption in the outflowing gas results in the weakening of the mass flux $J = \varrho_b v_b R^2$ dependence on the primary X-ray intensity F_{x0}. For the monochromatic X-ray flux the plasma density ϱ_b at the point b was estimated above (cf. Equation (31)). For the low X-ray intensity $\varrho_b \propto F_{x0}$ and for the high one $\varrho_b \propto \sqrt{F_{x0}}$. The flow velocity v_b depends on the temperature T_b only, which is a weak function of the X-ray intensity. As a result $J = \varrho_b v_b R^2 \propto F_{x0}$ for a small X-ray flux and $J \propto \sqrt{F_{x0}}$ for a large one.* A similar result was obtained earlier [36] for the motion of the ioniza-

* For small values of F_{x0} (as numerical calculations show) the flow velocity V_b increases with increasing F_{x0} and T_b, the mass flux J being more strongly dependent on F_{x0} than directly proportional.

tion front with a large optical depth for ultraviolet radiation of the gas outflowing from it. The weakening of the dependence $J(F_{x0})$ and decreasing of the feedback coefficient result in a stabilizing of the outflow and X-ray luminosity at the level, determined by the X-ray spectrum, the parameters of the binary system and the efficiency of the energy release in accreting matter.

For stars with smaller gravity acceleration the flow becomes saturated at a smaller X-ray flux. The mass flow is essentially influenced by the soft part of the X-ray spectrum, so that the effect under discussion holds good for the broad X-ray spectrum as well. It is possible that for many of the X-ray sources entering binary systems with $L_x < L_c$ this autoregulation mechanism sets up an upper limit on their X-ray luminosity.

In Figure 9a the dependence of the mass loss rate $Q_e(L_x) = -\mathrm{d}\mathscr{M}/\mathrm{d}t$ of the normal star on the X-ray source luminosity L_x is presented for given parameters of the binary system. For small L_x the induced outflow makes a negligible contribution and $Q_e(L_x)$ asymptotically tends to Q_{net} – the stellar wind typical for the star considered when it is not irradiated with X-rays.

The dependence $L_{xe}(Q)$ – the X-ray source luminosity – on the mass loss rate Q of the normal component is given in Figure 9b. For small Q the X-ray luminosity $L_x = \alpha\eta Q c^2 \propto Q$, where α is the fraction of the mass flow captured by the relativistic object, η is the efficiency of reprocessing of the gravitational energy of the accreting matter into X-ray flux. For large Q the X-ray luminosity tends to the Eddington limit. The self-consistent regime of the mass outflow from the normal component and accretion onto the compact object is represented by the intersection points of curves $Q_e(L_{xi})$ and $L_{xe}(Q_i)$ when they are plotted at the same diagram with the appropriate coordinate axes reorientation (see Figure 9c). The state of equilibrium corresponding to this self-consistent regime is stable for $(\mathrm{d}Q_e(L_x)/\mathrm{d}L_x)/(\mathrm{d}L_{xe}(Q)/\mathrm{d}Q)_{Lx=Lxi,\ Q=Qi} < 1$ and unstable for the opposite case.* Depending on the binary system parameters, the X-ray spectrum and the efficiency of the energy release in accreting matter, there can be one (curves *a* and *e* in Figure 9c) or three (the curve *c*) states of equilibrium. The single state of equilibrium is always stable. The curve *a* represents detached binary systems, when a small fraction of the stellar wind is captured by the compact object, and the reaction of the X-ray source on the normal star is small. The curve *e* corresponds to the opposite case of the close binary system. In the intermediate case (the curve *c*) one of the three states of equilibrium L_{x2} is unstable when the other two (L_{x1} and L_{x3}) are stable. The curves *b* and *d* correspond to the degenerate cases when two of the states of equilibrium merge into an unstable one. The curves $Q_e(L_x)$ plotted in Figure 9c may represent the successive evolutionary stages of the normal star: the variation in radius and its other parameters. On these curves it is easy to trace the corresponding evolution of L_x. The effects of hysteresis type are evident: the turning-on of the maximal power of the X-ray source occurs at a larger stellar radius than the turn-off.

* The condition of stability may be easily obtained from the system of differential equations describing the behaviour of the system at small deviations from the state of equilibrium.

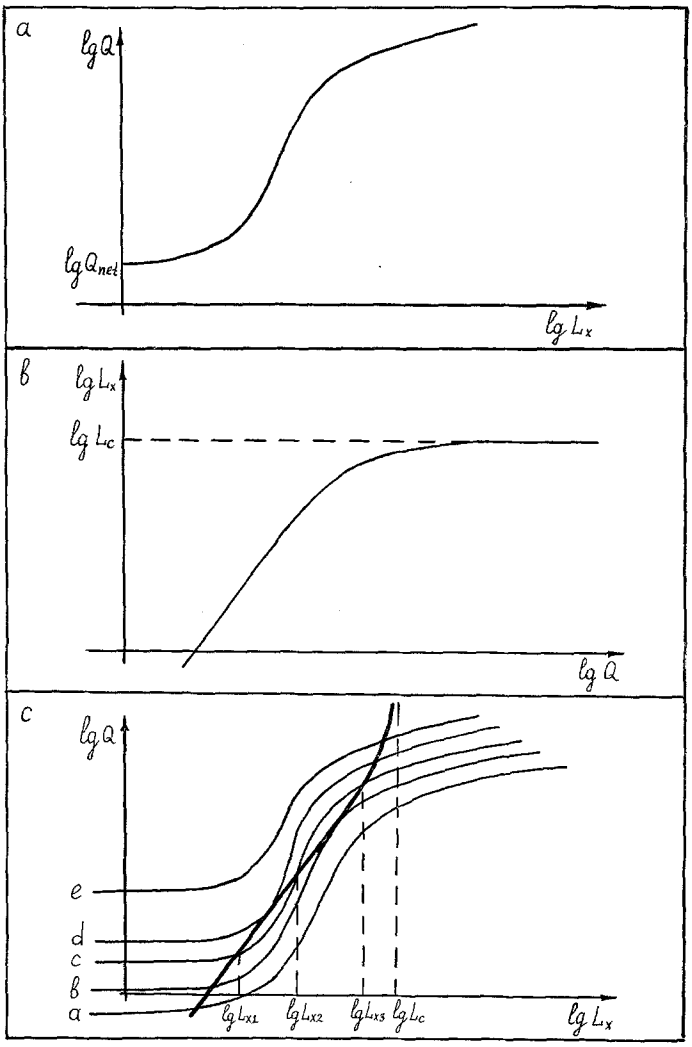

Fig. 9. The retroaction of the mass outflow on the X-ray luminosity L_x in binary systems: 9a – the dependence of the mass loss rate $Q_e(L_x) = -\mathrm{d}\mathscr{M}/\mathrm{d}t$ of the normal component on L_x; 9b – the dependence of X-ray luminosity $L_{xe}(Q)$ on the mass loss rate of the normal star Q; 9c – the curves from Figure. 9a and 9b are plotted together; the points of intersection represent the self-consistent regimes; depending on parameters of the binary system, X-ray spectrum and the efficiency of the energy release by accretion one of the five cases presented should occur.

5.2. THE MASS TRANSFER IN CLOSE BINARY SYSTEMS

The presence of inner Lagrangian point affects the mass outflow from the normal component irrespective of whether the star fills its Roche lobe or not. The simple estimates given below illustrate the causes of the mass outflow increase.

We shall introduce the corotating coordinate system $OXYZ$, the origin O coinciding with the centre of the normal component, the X-axis passing through the centres

of both components and the XY plane coinciding with the plane of the orbit (see Figure 10). The acceleration of the particle being at rest at the distance r from the centre of the normal star along the X-axis is given by

$$g(r) = \frac{G\mathcal{M}}{r^2} - \gamma \frac{G\mathcal{M}}{(A-r)^2} - \Omega^2\left(r - \frac{A}{1+\gamma}\right), \tag{38}$$

where $\gamma\mathcal{M}$ is the mass of the X-ray source, A is the distance between the component centres, $\Omega = \sqrt{(G\mathcal{M}(1+\gamma)/A^3)}$ is the angular velocity of the orbital motion. The acceleration $g(r)$ varies rapidly only immediately near the inner Lagrangian point r_1 where $g(r_1) = 0$.

The structure of the star with dimensions close to those of its Roche lobe is strongly affected by the gravity acceleration distribution as given by Equation (38). The stellar atmosphere may be calculated along the arbitrary radius according to the usual formulae (for given g) until

$$H \ll \left|\frac{\mathrm{d}}{\mathrm{d}r} \ln g(r)\right|^{-1}. \tag{39}$$

where H is the uniform atmosphere height. All this is valid in the direction towards the compact counterpart. It should be noted that in this direction the most important is the rapid decrease of g near Lagrangian point, but not the dependence of H on T, $\mathcal{M}$ and R.

Let the condition (39) be fulfilled for the hot gas in bc region too. Equation (31) shows that the density at the point b is not sensitive to the variations of H and, con-

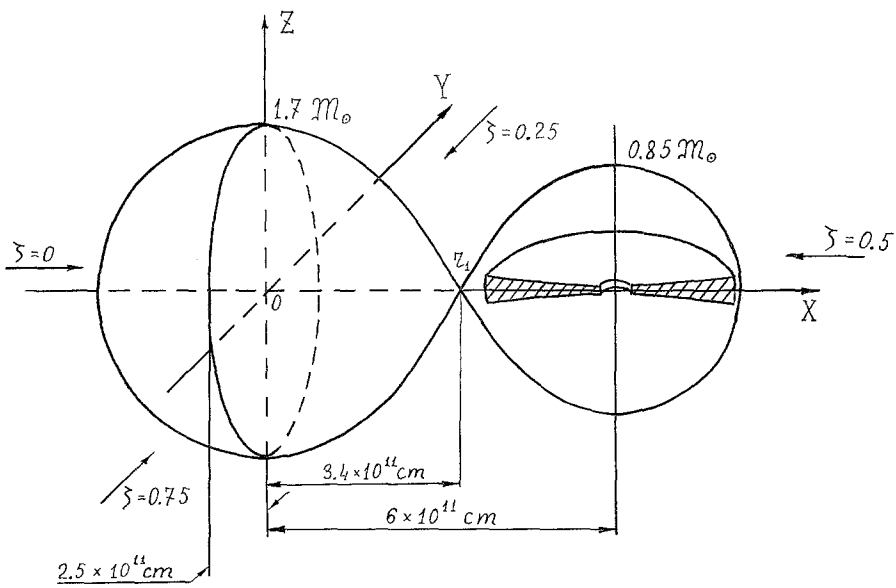

Fig. 10. The parameters of HZ Her = Her X1 system.

sequently, of $g \propto 1/H$. The increase of H affects most strongly the mass flow towards the Lagrangian point (cf.(33)). The critical point draws nearer to the stellar surface. The height $H(r_b)$ being much less than R for a single star, the flow velocity v_b and the mass flux towards Lagrangian point in the binary system may exponentially increase

The stellar surface being closer to Lagrangian point, the condition (39) may be violated in the jump region *ab*. The dense layers are then set in motion and the mass flow increases. Conventionaly, just the case of the star filling its Roche lobe is discussed in the literature [37]–[39]. The condition (39) is then violated in the photosphere already, and the mass outflow is significant irrespective of the X-ray flux influence.

To evaluate the mass loss rate J_{12} through Lagrangian point, one should find the velocity and the effective cross section of the flow.

5.2.1. *The Flow Velocity at Lagrangian Point*

The second equation from (2) for the narrow spherical sector along X-axis, the Coriolis force being neglected, now becomes

$$v\frac{\mathrm{d}v}{\mathrm{d}r}+\frac{1}{\varrho}\frac{\mathrm{d}p}{\mathrm{d}r}+\frac{G\mathscr{M}}{r^2}-\gamma\frac{G\mathscr{M}}{(A-r)^2}-\Omega^2\left(r-\frac{A}{1+\gamma}\right)=0. \tag{40}$$

Restricting ourselves as earlier to the isothermal flow, instead of (7) we now obtain the following equation for the critical location point r_c

$$\frac{1}{\xi_c^2}=\frac{\gamma}{(1-\xi_c)^2}+\frac{4v_s^2}{v_p^2}\frac{1}{\xi_c}+\xi_c(1+\gamma)-1, \tag{41}$$

where $\xi_c=r_c/A$, $v_s^2=\mathscr{R}T/\mu$, $v_p^2=2G\mathscr{M}/A$. For the inner Lagrangian point $\xi_1(\gamma)=r_1/A$ we have

$$\frac{1}{\xi_1^2}=\frac{\gamma}{(1-\xi_1)^2}+\xi_1(1+\gamma)-1. \tag{42}$$

From Equations (41) and (42) we find that always $\xi_c<\xi_1$. It means that the flow passes through the Lagrangian point with a supersonic velocity. Since the velocity of the supersonic flow varies slowly with the distance (cf. Equation (32)), we shall adopt the flow velocity at Lagrangian point as being equal to v_s. The above analysis is performed for a spherical streamtube towards the compact component. However, the final result does not depend on this assumption. In case of a cylinder streamtube the second term in the right part of Equation (41) is absent and the critical point coincides with the inner Lagrangian point r_1. A similar result was obtained in [38]. It should be noted that the Coriolis force may be neglected for $v_s \ll v_p$. For the sake of simplicity we shall assume that this condition is always fulfilled.

5.2.2. *Effective Cross-Section of the Flow*

With the aid of Equation (40) the mass flux per unit solid angle at Lagrangian point and the density distribution along the X-axis may be evaluated. In a real situation due to the gas pressure the jet at Lagrangian point has finite dimensions determined by the gas temperature and gravitational forces. We shall assume that the velocity of the

gas crossing a plane perpendicular to X-axis near Lagrangian point is parallel with X-axis, and the temperature is constant in this plane. Then two of the three hydrodynamical equations turn to be those of hydrostatical equilibrium [38]

$$\begin{aligned} \frac{\mathscr{R}T}{\mu}\frac{\partial \varrho(y,z)}{\partial y} &= \varrho(y,z)\frac{\partial \Psi(y,z)}{\partial y}, \\ \frac{\mathscr{R}T}{\mu}\frac{\partial \varrho(y,z)}{\partial z} &= \varrho(y,z)\frac{\partial \Psi(y,z)}{\partial z}, \end{aligned} \tag{43}$$

where $\psi(y, z)=G\mathscr{M}[r_1^2+y^2+z^2]^{-1/2}+\gamma G\mathscr{M}[(A-r_1)^2+y^2+z^2]^{-1/2}+\Omega^2y^2/2$ is the potential of centrifugal and gravitational forces. Integrating (43) and keeping first terms of the $\psi(y, z)$ expansion near Lagrangian point we obtain

$$\begin{aligned} J_{12} &= v_s\int_{-\infty}^{+\infty}\int_{-\infty}^{+\infty}\varrho(y,z)\,dy\,dz = \pi A^2\varrho_1 v_s(v_s^2/v_p^2)\,\psi(\gamma) = \\ &= 3.53\times 10^{-6}\,\varrho_1 T^{3/2}P^2\mu^{-3/2}(1+\gamma)\,\psi(\gamma)\,\mathscr{M}_\odot\ \mathrm{yr}^{-1}, \end{aligned} \tag{44}$$

where ϱ_1 is the plasma density at Lagrangian point, P is the orbital period of the system in days and

$$\psi(\gamma)=[\xi_1^{-3}+\gamma(1-\xi_1)^{-3}]^{-1/2}\{\xi_1^{-3}-1+\gamma[(1-\xi_1)^{-3}-1]\}^{-1/2} \tag{45}$$

is a slowly varying function ($\psi(0.1)=0.152$, $\psi(1)=0.067$, $\psi(10)=0.015$). The expansion of $\psi(y, z)$ near $(r_1, 0, 0)$ for binary system is equivalent to the exponential atmosphere approximation for a single star. From Equation (44) we can see that the effective flow cross-section is proportional to the gas temperature. The X-ray heating results in an increase of the mass outflow through the Lagrangian point. The expression for J_{12} obtained above can be used in the case of the star filling its Roche lobe, when the approximate description of the outflowing atmosphere breaks down. In this case some other speculations are necessary to evaluate ϱ_1 and T.

In the HZ Her-model (Section 6.1.) the height of the isothermal atmosphere in bc region is close ($\sim\frac{1}{3}$) to the Roche lobe radius. The flow velocity at the point b is insensitive to the presence of the second component, the gravitational attraction of which increases the mass flux at Lagrangian point by no more than twice (compared to the calculations for a single star). It is possible that the surface of HZ Her is just near Lagrangian point and the condition (39) breaks down in the jump region. Then the gas in the flow is relatively cold and dense, the soft X-rays ($h\nu\sim 1$–5 keV) being effectively absorbed in it. The autoregulation similar to the one considered above (Section 5.2.) should take place in this case too. When the condition (39) breaks down in the photosphere the mass outflow increases merely due to T_{eff} exceeding over T_0 (cf. (44)).

5.3. Optical appearances

In a binary system the X-rays illuminate one side of the star only. Let the whole solid

angle at which the normal component is visible from the X-ray source (point C in Figure 11) be illuminated with X-ray radiation. How does the brightness of the system varies with the variations of the observation phase and the inclination of the orbit?

5.3.1. *Limb Darkening*

If the normal component is a spherical star of radius R then the X-ray flux falling per unit stellar surface area is given by

$$\cos\psi \int_0^\infty \mathscr{F}_x(\nu, R)\,\mathrm{d}\nu = \alpha(\vartheta)\,\mathscr{L}_x \cos\psi/l^2\,, \tag{46}$$

where

$$\alpha(\vartheta) = \frac{l^2}{\mathscr{L}_x}\int_0^\infty \mathscr{F}_{x0}(\nu)\exp\left[-\tau_x(\nu, R)\sec\psi\right]\mathrm{d}\nu\,. \tag{47}$$

is the fraction of the X-ray flux penetrating within the photosphere. Here $\mathscr{L}_x = l^2\int_0^\infty \mathscr{F}_{x0}(\nu)\mathrm{d}\nu$ is the averaged over the pulsational period X-ray luminosity per unit solid angle (in case of isotropically radiating X-ray source the total luminosity $L_x = 4\pi\mathscr{L}_x$), $\tau_x(\nu, r) = x_H/m_p\int_r^\infty \varrho(r)\sum c_i(r)\sigma_i(\nu)\mathrm{d}r$ is the optical depth for X-rays with respect to photoabsorption along the radius, $l^2 = A^2 + R^2 - 2AR\cos\vartheta$, $\cos\psi = (A\cos\vartheta - R)/l$ (see Figure 11). Since X-rays are mainly absorbed near the photosphere, the atmosphere at every surface point may be treated as plane-parallel. For the hard X-ray spectrum ($kT_x \sim 10$–15 keV) $\alpha(\vartheta)$ slowly varies with ϑ, for $\tau_x(\nu, R) \ll 1$ and $\mathscr{F}_{x0} \propto l^{-2}$. The stellar surface temperature at every point (ϑ, R) is given by

$$T_{\mathrm{eff}}^4(\vartheta) = \begin{cases} T_0^4 + \mathscr{L}_x\alpha(\vartheta)\cos\psi/bl^2\,, & R/A < \cos\vartheta \leqslant 1 \\ T_0^4\,, & -1 \leqslant \cos\vartheta \leqslant R/A\,. \end{cases} \tag{48}$$

From the unit surface area per unit solid angle towards the observer the energy flux $bT_{\mathrm{eff}}^4\cos\delta/\pi$ is radiated, where

$$\cos\delta = \cos\Theta\cos\vartheta + \sin\Theta\sin\vartheta\cos\varphi\,, \tag{49}$$

and such a coordinate system is chosen (see Figure 11) that the line of observation is parallel to EOC plane and makes an angle Θ with OC axis.

The hottest point A with the temperature $T_1 = T_{\mathrm{eff}}(0)$ lies on the line of centres ($\vartheta = 0$). With the increase of ϑ the surface temperature drops (cf. Equation (48)) for three reasons: due to the X-ray dilution ($\mathscr{L}_x/l^2 \leqslant \mathscr{L}_x/(A-R)^2$), the oblique incidence of X-rays ($\cos\psi \leqslant 1$), and the additional X-ray absorption in the optically thin for optical frequencies region ($\alpha(\vartheta) \leqslant \alpha(0)$). As a result, the area illuminated by the X-rays has a more sharp than the normal star limb darkening. For $T_1 \gg T_0$, $A \gg R$ and $\Theta = 0$ the limb darkening is proportional to $\cos\vartheta$, and even more sharp for $A \sim R$.

5.3.2. *Optical Variability*

The total energy flux per unit solid angle radiated by the normal star towards the

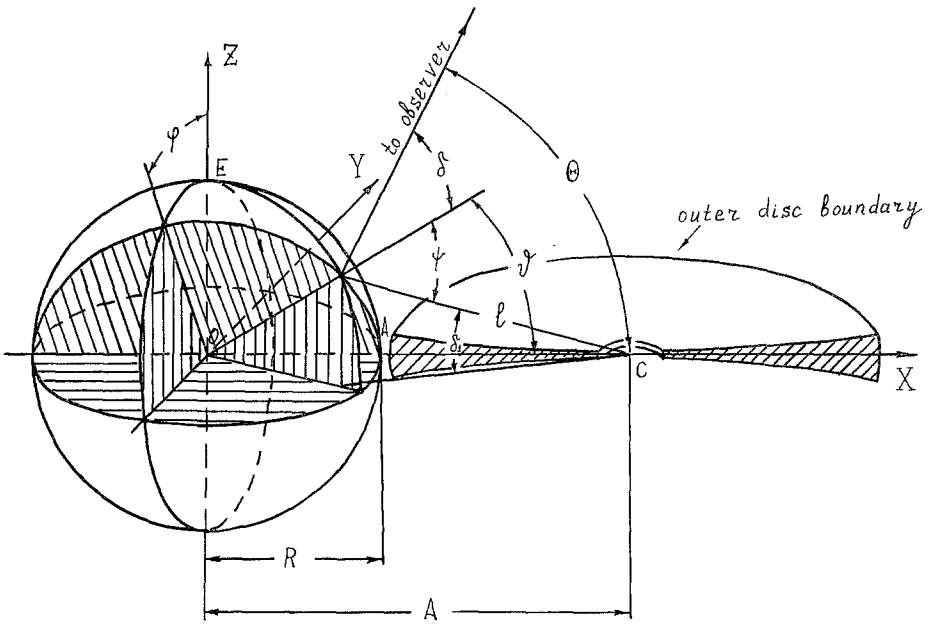

Fig. 11. The geometry of the binary system.

observer is

$$\mathscr{L}_b(\Theta) = \frac{R^2}{\pi} \int_0^{2\pi} \mathrm{d}\varphi \int_{\cos\vartheta_1}^{\cos\vartheta_2} bT_{\mathrm{eff}}^4 \cos\delta \mathrm{d}\cos\vartheta, \tag{50}$$

where

$$\cos\vartheta_1 = \begin{cases} -\dfrac{\sin\Theta\cos\varphi}{\sqrt{1-\sin^2\Theta\sin^2\varphi}}, & 0 \leqslant \Theta \leqslant \pi/2 \\ -1, & \pi/2 \leqslant \Theta \leqslant \pi \end{cases}$$

$$\cos\vartheta_2 = \begin{cases} 1, & 0 \leqslant \Theta \leqslant \pi/2 \\ \dfrac{\sin\Theta\cos\varphi}{\sqrt{1-\sin^2\Theta\sin^2\varphi}}, & \pi/2 \leqslant \Theta \leqslant \pi. \end{cases} \tag{51}$$

It will be convenient to introduce the quantity

$$I(\Theta) = \frac{\mathscr{L}_b(\Theta)}{R^2 bT_0^4} = \frac{1}{\pi} \int_0^{2\pi} \mathrm{d}\varphi \int_{\cos\vartheta_1}^{\cos\vartheta_2} (T_{\mathrm{eff}}^4/T_0^4) \cos\delta \mathrm{d}\cos\vartheta. \tag{52}$$

The optical variability of the system results from its rotation. The X-ray illuminated area of the normal star for $\sin i \sim 1$ periodically proves to be out of sight (eclipsed). The optical brightness of the system should then have a plateau at minimum with the angular width equal to that of the X-ray eclipse*. The bolometric magnitude varies

* For the star filling its Roche lobe the gravity darkening significantly affects the surface temperature distribution of the area of the star which is not illuminated by X-rays. For this reason the minimum may be observed instead of the plateau.

according to

$$m_b = m_{b0} - 2.5 \lg \{I[\arccos(-\sin i \cos 2\pi\zeta)]\}, \tag{53}$$

where $0 \leqslant \xi \leqslant 1$ is the phase of observation (the phase $\xi = 0$ coincides with the middle of the optical plateau and X-ray eclipse), m_{b0} is the bolometric magnitude of the normal component, the X-ray flux being absent (see Figure 1e). For $i = 0$ the brightness variations are absent. The characteristic feature reflecting the presence of the hot spot on the stellar surface will be in this case the complex spectral class of the star – i.e., lines of different spectral types should be observed. The possibility is of interest that absorption lines corresponding to the star itself and emission lines of the hot spot may be observed simultaneously. For $0 < i < \arccos(R/A)$, partial eclipses of the hot spot should be observed, appearing as a variability in lines and continuum with a smaller ($\propto \sin i$) amplitude than for $i = \pi/2$.

For a determination of the visual magnitude m_{pv} one can no longer use the known bolometric corrections because of the strongly variable surface temperature.

The spectral energy flux f_{pv} on Earth at a wavelength $\lambda = 5400$ Å is given by

$$f_{pv}(\Theta) = 2.6 \times 10^8 \frac{R^2}{D^2} \int_0^{2\pi} \mathrm{d}\varphi \int_{\cos\vartheta_1}^{\cos\vartheta_2} \frac{\cos\delta \, \mathrm{d}\cos\vartheta}{\exp[2.67 \times 10^4 / T_{\mathrm{eff}}(\vartheta)] - 1} \frac{\mathrm{erg}}{\mathrm{cm}^2 \, \mathrm{s} \, \text{Å}}, \tag{54}$$

where D is the distance of the system. The temperature $T_{\mathrm{eff}}(\vartheta)$ is determined from Equation (48). Analogous formulae can be written down for the star in a form of the ellipsoid of rotation. In Figure 1b the light curve is plotted according to Equation (54).

5.3.3. *Line Emission*

Lines are formed in the region ($\bar{\tau} < \frac{2}{3}$) which is optically thin for optical radiation. The non-saturated lines are radiated almost isotropically. Even for this reason only the ratio of the flux radiated in lines $\mathscr{L}_l(\Theta)$ to the flux in continuum $\mathscr{L}_b(\Theta)$ must increase with the increase of Θ from 0 to $\Theta_{\max}$, the latter depending on the surface temperature distribution. When $T_1^4 \gg T_0^4$ the angle $\Theta_{\max}$ tends to $\pi/2 + \arccos(R/A)$. The increase in ϑ is followed with a more oblique incidence of the X-rays. A smaller fraction of X-ray flux penetrates then within the photosphere because of the additional absorption in the optically thin region (the path is proportional to $\Delta r/\cos\psi$). The part of the X-ray energy flux absorbed and reemitted in the optically thin for the optical radiation region increases by

$$\beta_l(\vartheta) = \frac{\mathscr{L}_x[1 - \alpha(\vartheta)] \cos\psi}{bT_0^4 l^2 + \mathscr{L}_x \alpha(\vartheta) \cos\psi}. \tag{55}$$

6. Particular Systems

6.1. HZ HER = HER X1 SYSTEM

The phenomena discussed above are most pronounced in the binary system including the

eclipsing variable X-ray source Her X1 and the variable star HZ Her. The X-ray source is most likely a magnetic neutron star radiating due to the accretion of the outflow of the matter of the normal component. The X-ray pulsations apparently result from the neutron star gyration, the X-ray radiation being extremely beamed. The accretion to magnetic pole regions [39a] and cyclotron radiation of the hot ($T \sim 10^9$ K) plasma may account for such a beaming. In the case of isotropic electron velocity distribution they radiate at high harmonics of the gyrofrequency $\nu_H = eH/2\pi m_e c$ and the knife radiation pattern is formed. In another possible case when the electrons in a shock wave are relativistic $E_e = \Gamma m_e c^2$ and move at small pitch angles with respect to the magnetic field, they radiate mostly in the direction of their motion at a Doppler-shifted gyrofrequency $\nu = 2\Gamma\nu_H$ and the pencil radiation pattern appears with the angular width $\chi \sim 1/\Gamma \sim \nu_H/\nu$[40].

6.1.1. *Parameters of the System*

For the X-ray star the following data were obtained by observations: the orbital period of the system is $P = 1^d.7$; the X-ray pulsation period $p = 1.24$ s; the mass-function $f = \mathcal{M} \sin^3 i/\mathcal{M}_\odot (1+\gamma)^2 = 0.85$ ($\gamma\mathcal{M}$ is the X-ray source mass); the orbital radius of the X-ray source $a_x = A_x/\sin i = 4 \times 10^{11}$ cm/sin i; and the maximum angular width of the X-ray eclipses $50^\circ.8 < 2b_x < 63^\circ.8$[5]. The optical brightness of the system varies ($\Delta m_{pv} \approx 1^m.4$) with the same period $p = 1^d.7$. The spectral class changes simultaneously from G3–A7 up to B2–B5 [17], [41], [10]. The optical brightness minimum coincides in phase with the X-ray eclipse. The maximum brightness and the earliest spectral type are shifted in phase by 180° with respect to the minimum. Using the expression for the X-ray width of the eclipse

$$R_v^2/A^2 = 1 - \sin^2 i \cos^2 b_x, \tag{56}$$

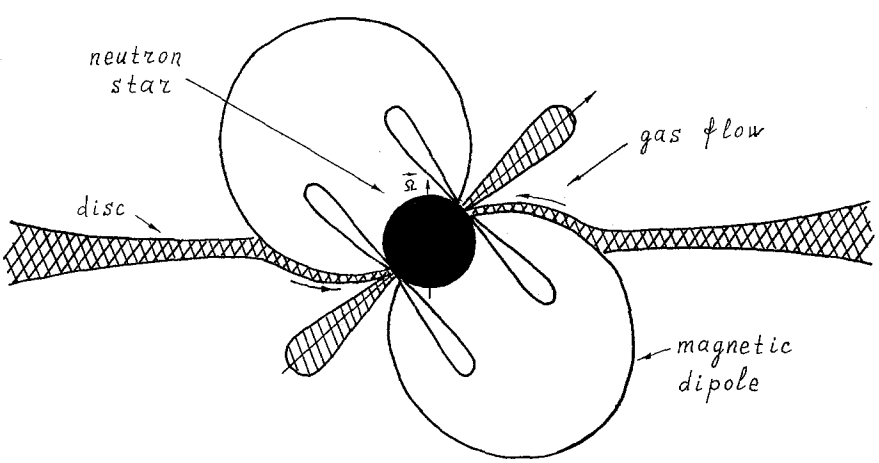

Fig. 12. The disc accretion of matter to the magnetic rotating neutron star. Schematically the inner disc boundary and a possible pattern of the mass flow to the magnetic pole regions are shown; the possible X-ray radiation patterns – knife and pencil – are presented (the latter is hatched).

and adopting $R_v \leqslant A\eta(\gamma)$, we readily obtain the estimates for component masses

$$\eta(\gamma) \geqslant \sin b_x, \quad \text{or} \quad \gamma \leqslant 0.55$$
$$\frac{\mathcal{M}}{\mathcal{M}_\odot} \leqslant f \frac{(1+\gamma)^2 \cos^3 b_x}{[1-\eta^2(\gamma)]^{3/2}} \leqslant 3.26 f \cos^3 b_x \leqslant 2. \tag{57}$$

where R_v and $A\eta(\gamma)$ are the minimum equatorial radii of the normal star and its Roche lobe. The function $\eta(\gamma)$ was calculated in [42], [43]. In [43] the approximate expression applicable for $0.1<\gamma<1$ is given by

$$\eta(\gamma) = 0.38\, \gamma^{-0.208} \tag{58}$$

The second inequality in (57) is valid for $0.02<\gamma<0.55$. For $b_x = 31\overset{\circ}{.}8$ the restrictions in (57) turn out to be more stringent: $\gamma \leqslant 0.21$ and $\mathcal{M}/\mathcal{M}_\odot \leqslant 1.25$, when $\gamma > 0.1$. For more precise determination of the system parameters along with the radial velocity measurements the more precise value of the eclipse duration should be obtained. From the mass function definition and (57) we have

$$1 \geqslant \sin i \geqslant \sqrt{1-\eta^2(\gamma)}/\cos b_x. \tag{59}$$

Since $A = A_x(1+\gamma)/\sin i$ and in virtue of (56) and (59) we find that

$$A_x f^{-1/2} \left(\frac{\mathcal{M}}{\mathcal{M}_\odot}\right)^{1/2} \frac{\sin b_x}{\cos^{1/2} b_x} [1-\eta^2(\gamma)]^{1/4} \leqslant$$
$$\leqslant R_v \leqslant A_x \cos b_x \frac{(1+\gamma)\eta(\gamma)}{[1-\eta^2(\gamma)]^{1/2}}. \tag{60}$$

The analysis of the above restrictions shows that the size of the visible star greatly exceeds those of the Main Sequence stars of the same mass, and most likely the normal component fills its Roche lobe [10]. We adopt the following stellar parameters (see Figure 10): $\gamma = 0.5$, $\mathcal{M} = 1.7\mathcal{M}_\odot$, $i \sim 80°$, $A = 6 \times 10^{11}$ cm, $R_v = 2.5 \times 10^{11}$ cm. If the X-ray eclipse half-width regularly varies within the interval $19° \leqslant b_x \leqslant 25\overset{\circ}{.}4$ [5] then the variations in radius of the star ($\pm 10\%$) may take place.

The analysis of the old plates (1932–1940 yr.) [44] revealed the strong optical variability of HZ Her with the period 1^d7 having been absent for some yr. the star having been not illuminated with X-rays. It is important that the light curve in this period is similar to that in Figure 1a with the amplitude being equal to $0^m\overset{m}{.}3$. These light variations can be easily explained with the ellipsoidal form of the star, the latter being an additional evidence for the star having filled its Roche lobe. Small deviations from the theoretical light curve most likely are accounted for by the gravity darkening.

6.1.2. *The Distance of the System and its Luminosity*

The latest spectral type should correspond to the star itself not subjected to the X-ray source's influence. Adopting it to be F5($T_{\text{eff}} \sim 6500$ K) and the visual magnitude at minimum being equal to $m_{pv} = 14\overset{m}{.}6$, we obtain the own luminosity of the normal component $L_v \approx 22 L_\odot = 8.4 \times 10^{34}$ erg s^{-1}. The interstellar absorption being neglected the distance of the system may be estimated at $D \approx 4$ kpc. HZ Her system has a high

galactic latitude ($b \approx 35°$), and for such distance value obviously is out of the galactic plane, possibly belonging to the halo [9], [45]. The distance being known, we can evaluate the averaged over the pulsational period X-ray luminosity of Her X1 per unit solid angle $\mathscr{L}_x = f_x D^2 \approx 7 \times 10^{35}$ erg s^{-1} ster^{-1} (the X-ray data presented in [16] were used). The total X-ray luminosity for the knife radiation pattern with the angular width 2χ equals then $L_x = 4\pi \mathscr{L}_x (p/\Delta p) \sin\chi \approx 10^{37} (p/\Delta p) \sin\chi$ erg s^{-1} where $(p/\Delta p) \sin\chi \leqslant \pi/2$. It should be noted that the range 2–6 keV contains only a small fraction of the total energy flux, the major part being transmitted with the photons of $h\nu \sim 10$–30 keV.

The earliest spectral type is that of the hot-spot centre. Adopting it to be $B3 (T_{\text{eff}} \sim \sim 16000$ K) and assuming $\alpha(\vartheta) = 0.8$ (see Section 2.3.) we obtain another estimate of the X-ray luminosity $\mathscr{L}_x \approx 3 \times 10^{35}$ erg s^{-1} ster^{-1}. It should be noted that, depending on the orientation of the magnetic axis and the axis of the neutron star rotation and the radiation pattern properties, the averaging over the X-ray pulsations on Earth may give the results differing from those on HZ Her surface. The comparison of these estimates shows that Her X1 is luminous enough to raise the temperature at HZ Her surface up to 16000 K and even higher.

6.1.3. *Reflection of Hard X-rays by the Stellar Surface*

The Compton scattering cross-section σ_T for $h\nu > 8$ keV exceeds that of the photoabsorption in the gas with normal chemical abundances (and this relationship is independent of the ionization degree, for $h\nu \geqslant \chi_{\text{H}}$ – the ionization potential of hydrogen) [46], [30]. In the case of Her X1 source the major part of the energy is radiated with energetic photons $h\nu \sim 15$–30 keV [47]. They are scattered in the atmosphere of the normal component, and a considerable part (20–60%) [48] leaves the atmosphere unabsorbed, being scattered a few (<20) times. In every act of scattering photons lose a small part of their energy $\sim h\nu (h\nu/m_e c^2) \gg \chi_{\text{H}}$ ionizing and heating the electrons through the recoil. The photoabsorption cross-section is small $\sigma \propto v^{-3}$ for $h\nu \sim 15$–30 keV, so that the recoil effect plays a significant role in the X-ray energy absorption. Thus, the scattering with the recoil and the photoabsorption taken into account results in about 70% of the incident X-ray energy being absorbed and the other 30% being diffusively reflected [25a].

The dependence of the intensity of the reflected X-rays on the phase of observation should be similar to the bolometric light curve (Figure 1e). The eclipses in reflected X-rays should be wider than the X-ray source eclipses. Even more interesting is the fact that reflected X-rays are not beamed and should be observed on Earth for those 24 days of 36 when the X-ray beam does not intercept the Earth. The ratio of the intensity of the reflected X-ray flux at phase $\xi = 0.5$ to the maximum X-ray intensity over 36-day cycle equals to $R^2 \int_{R/A}^{1} (\cos\psi \cos\vartheta / l^2) \mathrm{d}\cos\vartheta \approx 0.1$. Perhaps both these effects were observed by OSO-7 [16].

The reflected X-ray flux should pulsate with a smaller ($\sim 10\%$) amplitude with the period 1.24 s, because of the large stellar radius ($R/c \gg p$). The signal reflected by different parts of the stellar surface comes to the observer with the phase difference exceeding the pulse duration [25a].

The reflection of hard X-rays by the surface of the normal component makes it possible to search for the X-ray pulsars the beam of which never covers the Earth. Such sources should be observed in the hard X-rays only with the soft X-rays spectrum interval being cut off at $h\nu < 10$–15 keV.

6.1.4. *Model of the System*

Assuming that the X-ray transformation in the atmosphere of HZ Her accounts for the system variability we can easily obtain the theoretical light curve according to Equation (54) for the above adopted parameters of the system (Section 6.1.1.). The result (Figure 1b) is not consistent with the observational data (Figure 2a) and indicates that the theoretical model is inadequate. The theoretical light curve is much more narrow than the observed one. The above predicted plateau at minimum light is absent. Moreover, the minimum shape suggests the occultations of the extended object with the luminosity comparable to that of the star itself.

The disc of matter accreting to the neutron star may be such an occulting object. The matter flows through the inner Lagrangian point and is captured with the gravitational field of the compact component. Due to the angular momentum it cannot directly fall onto the neutron star and moves along quasi-keplerian orbits. The viscosity causes the slow radial motion of the orbiting matter to the gravity centre. Eventually, the thin ($h/r_x \ll 1$) disc of accreting matter is formed [4]. At the inner boundary of the disc ($r_x \sim 10^7$–10^9 cm) the magnetic field of the neutron star $H^2/8\pi \sim \gamma G\mathcal{M}\varrho h/R_1^2$ significantly affects the motion of the accreting matter. Here h is the disc thickness, ϱ is the plasma density in it, R_1 is the distance of the inner disc boundary from the neutron star [22], [24], [49]. The external disc radius may be of the order of that of the neutron-star Roche lobe.

The own optical luminosity of the disc due to the gravitational energy release [4] is small ($\lesssim 10^{-3} L_x$). Due to the small compared to the inner disc boundary $R_1 \sim$ ~ 30–10^3 R_{ns} radius of the neutron star R_{ns} X-rays emitted from the surface of the neutron star do not get onto the disc surface. The angle at which one sees the disc from the neutron star is also small namely, $\Omega/4\pi \sim h/r_x \sim 10^{-2}$ [4]. Therefore, the disc is not any obstacle for X-rays* emitted from the neutron star surface [40]. Its own X-ray luminosity is small too ($< (R_{ns}/R_1) L_x \approx 10^{-3}$–$3 \times 10^{-2}\, L_x$).

The disc will radiate reflecting and reemitting the optical, ultraviolet and hard X-ray radiation of the hot area of the visible star. The surface temperature of the disc is variable; along the X-axis (see Figure 9) it varies according to

$$T_d^4 = T_0^4 \frac{2\lambda^3}{\pi} \int_{\lambda}^{1} \left\{ 1 + \left(\frac{T_1^4}{T_0^4} - 1 \right) \frac{(1-\lambda_0)^2 (y-\lambda_0)}{(1+\lambda_0^2 - 2\lambda_0 y)^{3/2}} \right\} \frac{(y-\lambda)\sqrt{1-y^2}}{(1+\lambda^2-2\lambda y)^2}\, \mathrm{d}y \tag{61}$$

The optical spectral flux from the disc is $f_{pvd} = \cos i / D^2 v^2 / c \int_{s_d} B(\nu, T_d) \mathrm{d}s_d$ erg cm^{-2} s^{-1} Å^{-1}, where $\lambda = R_v/r$, $\lambda_0 = R_v/A$, $y = \cos\vartheta$ (see Figure 11) and R_v is the radius of the visible

* The absorption and transformation of X-rays by the disc does not influence the X-ray luminosity of the system, but it may be responsible for the optical luminosity of the disc $L_{\mathrm{opt}} \sim 10^{-2} L_x$ [4].

star. The temperature is maximum near the inner Lagrangian point, and minimum near the outer one. The evaluation of (61) shows the main part of the disc have the temperature 5000°–8000° K. At this temperature the maximum energy is radiated in the optical range 4000–7000 Å when at 16000° K it contains only 16% of the total energy flux. Therefore, the reemission of even a small part ($\lesssim 0.2$) of the radiation by the hot spot energy gives rise to disc radiation comparable with that of the visible star. Up to $\frac{1}{3}$ of the disc radiation is due to the reemission of the hard X-rays reflected by the stellar surface. However, primary X-rays are more important (see footnotes on the pages 121 and 149).

The disc radiation makes a considerable contribution to the luminosity of the system for large enough deviation of the inclination angle i from 90°. The observational data are fitted best of all for $i \approx 70°$–$80°$. We shall adopt $i = 75°$. In the phase $\xi = 0.5$ at maximum light the disc partly occults the hot spot at the visible star surface decreasing its brightness by 20–30%. At the same time an extra disc radiation increases the system brightness in the phases 0.25 and 0.75. Both these effects broaden the light curve. The occultations of the disc with the star account for the light curve shape near the minimum.

The observational data are best fitted with the following brightness distribution between the components – the hot spot (the phase 0.5, unocculted with the disc): the luminosity proper of the visible star (at the phase 0): the disc luminosity – 4:1:0.7. The estimates show that such a distribution is consistent with the parameters of the system adopted and X-ray energy supply by Her X1, which is responsible for the main part of the optical luminosity of the system. At maximum light ($I \approx 3.7$ in the luminosity scale adopted) the hot spot occultations ($\sim 25\%$) are to a great extent compensated with the proper radiation of the disc. In the phases 0.25 and 0.75 ($I \approx 2.4$) the disc luminosity is comparable with that of the star itself. The theoretical light curve is shown in Figure 2b.

The presence of the disc emission and absorption lines may cause some difficulties to the determination of the radial velocities of the normal component. The gas in the disc revolves around the neutron star and participates in the common orbital motion of the system. The hot spot area may rotate in phase with the X-ray source, i.e. in antiphase with the cold stellar side.

6.1.5. *Effects Connected with the Strong Directionality of X-Rays*

The observed X-ray radiation of Her X1 is modulated with the period 36 days [5]. The optical variability of HZ Her with the period $1^d.7$ connected with the X-ray reprocessing does not vanish during those 24 days of 36 when no X-ray flux from Her X1 is observed on Earth [44]. It undoubtedly indicates that X-rays do not cease to illuminate the star during those 24 days and justifies the idea of X-ray source precession*.

* It is possible, that the neutron star is not precessing, and the exit of the Earth from the radiation pattern is connected with the periodic narrowing and broadening of the latter [50]. The accretion rate variation causes the variation in parameters of the shock wave formed by accreting matter at the neutron star surface. The plasma temperature variation results in the variable angular width of the radiation pattern and variable X-ray spectrum [40]. In the case of precession there are no grounds for spectral variations.

The axis of the X-ray radiation pattern should periodically change its orientation [5], [8], [51] in such a way that the Earth could periodically exit of this pattern; the normal star being always illuminated with X-rays. The latter is not surprising, for the normal component is seen from the X-ray source at an angle exceeding 50°.

If X-ray source precesses, the brightest point may creep along the stellar surface, and that the closest to X-ray source point may be not illuminated by the X-rays. It should result in a phase shift and in a change of the stellar magnitude at maximum light (Section 5.3.). These effects may cause the periodical appearance of HZ Her light-curve asymmetry connected with the 36-day cycle (see Figure 2c, d). Such an asymmetry was detected by Kurochkin [25] from photographic observations. A shift of the hot spot along the stellar surface should be followed by variation, of the mass flow rate and connected with its variation in the X-ray luminosity.

For a high rate of the stellar mass loss the gas flow out of the Roche lobe may appear. The reemission of the optical and ultraviolet radiation of the hot spot may significantly affect the brightness of the system at minimum light, for they are not efficiently occulted with the star. It may also account for the observed periodical variation in the depth and shape of the minimum [25].

The sharp X-ray beam may cause the existence of the narrow boundary layer between the cold and X-ray-heated areas of the stellar surface. Convective motions and shock waves will blur this boundary. But they cannot effectively transfer the energy to the distances exceeding $v_s(T_{\text{eff}})\Delta t_c(R) \sim 10^7$ cm $\ll R$ (Δt_c is the characteristic radiative cooling time): the gas cools faster than it is transported to a significant distance moving with a speed close to that of the sound. Just for this reason the energy transfer to the shaded side of the star is also negligible.

6.1.6. *Excitation of Stellar Pulsations*

There are some reasons (the variation in the eclipse duration, 36-day cycle, etc.) to believe that the star periodically changes its size [5], [50]. Such pulsations may be excited by X-rays modulated with the 36-day cycle connected with the neutron star precession.

The X-rays may penetrate within the deep stellar layers ($\bar{\tau} \sim 100$), where the temperature is high enough to ionize helium atoms. This zone of helium ionization plays a crucial role in pulsational mechanism of the cepheids [52]. The instability mechanism being available, the periodical disturbances of the stellar atmosphere with the variable X-ray flux may cause the growth of the amplitude of the induced stellar pulsations.

6.1.7. *Optical Pulsations*

The X-ray pulsations with the period 1.24 s do not influence the mass outflow for the characteristic hydrodynamical time scale of $\sim 10^4$–10^5 s. But they may cause the optical pulsations with the same period. The time for which plasma radiates its energy may be estimated from the expression

$$\Delta t_c(r) = \frac{3}{2} \frac{\mathscr{R}T(r)}{\mu q^-(r)} = \frac{3}{2} \frac{\mathscr{R}T(r)}{\mu q^+(r)}, \tag{62}$$

where $q^+(r)=q^-(r)$ are taken from the steady-state solution. The expression (62) holds also for the optically thick zone $\bar{\tau}\gg 1$. For the model HZS (20) at the photosphere boundary $\Delta t_c(r_a)\sim 0.2$ s, $\Delta t_c(R)\sim 3$ s. In deeper layers where the main part of X-rays is absorbed, $\Delta t_c\sim 10$–20 s, and the optical pulsations should be weak. Since $R/cp>1$ (c is the velocity of light), their amplitude should be decreased by R/cp, for the different parts of the hot area radiate in different phases of X-ray pulses.

Attention should be drawn to the optically thin region where Δt_c is small and the energy is mainly radiated in lines. If the hot spot with $\Delta\vartheta R/cp<1$ radiates the main part of energy flux in lines, then the observed optical pulsations [41] may be connected with the line radiation. In this case the pulsations as well as lines should be most pronounced in the phases $\xi_1\sim 0.25$ and $\xi_2\sim 0.75$ (Section 5.3.3.). The connection of the pulsations with the line emission can be ascertained from the observations of the variability in individual bright lines.

The pulsating optical radiation may originate also near the X-ray source, in the region where the incident gas is stopped for instance by the neutron star magnetosphere [49]. In this case the optical pulsations should be the most pronounced just before and after the X-ray source eclipse when the total optical luminosity is small.

6.1.8. *Mass Transfer*

The numerical calculations for the model HZ (20) gave the mass-loss rate $J\approx 3\times 10^{-9}$ $\mathcal{M}_\odot$ yr^{-1} ster^{-1}. The solid angle ω at which the X-ray source Roche lobe is seen from the centre of the normal star should be close to $\omega\approx 0.3$. The rate of mass transfer is then estimated at $J_{12}\ 10^{-9}\ \mathcal{M}_\odot$ yr^{-1}. What does the influence of the second component alter? This question was discussed above in some detail (Section 5.2.). To illustrate this influence, we shall mention that when the normal star fills its Roche lobe by 80% the mass transfer rate is three times larger than the given above value.

The matter may flow out of the normal component in the form of a cold gas jet, or in the form of the hot gas flow. It is important for us that, in the latter case, for the normal star nearly filling its Roche lobe the matter flows mainly towards the X-ray source and the flow velocity is small compared with the parabolic velocity of escape from the system. The stellar wind reduces to a great extent to the mass transfer from the normal star to the compact one, the jet cross-section being broad and comparable to the dimensions of the system. A considerable amount of matter may flow in to the disc, but there is no doubt that more favourable conditions for disc formation occur when the cold and dense plasma flows out of the jump zone or immediately out of the photosphree (Section 5.2.), the filling-up of the Roche lobe being necessary for the latter case to take place.

The energy supply for the given above (Section 6.1.2.) value of X-ray luminosity needs an accretion rate 10^{-10}–10^{-9} $\mathcal{M}_\odot$ yr^{-1}. Thus, a considerable part of the outflowing matter may leave the system. Such a high value of the mass transfer rate in the system of HZ Her suggests a comparatively short time ($t\ll 10^8$ yr.) for the existence of the X-ray source. This time seems to be very short. It depends on the evolutionary time scale – time interval for which the normal component fills its Roche lobe.

The turn-off of the strong optical variability with the period $1^d.7$ for some yr [44] may be accounted for by: (1) the turn-off of the X-ray source, and (2) the normal star being not reached by the X-ray beam (variation in the X-ray radiation pattern). The latter may be due to the secular motions of the magnetic poles, the existence of the slow nutation or precession, etc. The case (2) is possible only when the star fills its Roche lobe and the gas flows out of the photosphere. The occultations by the cold disc of accreting matter result in a broader and deeper minimum at the phase 0.5 than at the phase 0 (and just that is observed [44]).*

However, more probable is the first possibility – a considerable decrease of the rate of mass – loss, and the turn-off of the X-ray source. The equal amplitude of the optical variability with the period $1^d.7$ before and after the turning off indicates, perhaps, that the above mentioned autoregulation mechanism takes place and Her X1 has the X-ray luminosity at the maximum level.

6.2. Sco X1 system

Shklovsky pointed out in 1967 [3] that the X-ray luminosity of Sco XI – the brightest X-ray sources – may be accounted for by the accretion of matter by the neutron star. The subsequent detailed spectral examinations of Sco X1 and of the optical object identified with it at different spectral intervals have led to the conclusion that Sco X1 is a single source radiating as an optically thin plasma cloud [53]. However, recent calculations of the spectrum of the discs formed by the accretion of matter by the black-hole [4], [22], [26] gave the spectral shape close to that of Sco X1. The observed X-ray and optical radiation in this case is a sum of the black-body spectra with different temperatures and radiated by the different parts of the disc. Rayleigh-Jeans spectrum in the infra-red range is formed at the outer cold disc boundary. In view of all this the following possibility is of interest. The source Sco X1 is a Schwarzschild black hole entering a binary system with $\sin i \approx 0$. The observational effects due to the binary nature are minimum in this case. The optical component is a cold star with the luminosity less than that of the disc $L_{opt} \ll 10^{-3} L_x$ [2].

Such a model leads to some restrictions on parameters of the system. Besides the own luminosity of the optical component L_1 being small ($L_1 \lesssim 10^{-4} L_x$), the fraction of the X-ray flux reemitted as the optical radiation in its atmosphere L_2 should also be small. For the latter, a small X-ray flux towards the normal component is of importance; the disc is optically thick and radiates mainly in the direction perpendicular to its plane ($\propto \sin \delta_1$, see Figure 11), with the result that a small fraction of the total X-ray flux falls on to the stellar surface. The mass outflow rate from the cold and compact component to be large, it is necessary for its size to be close to that of Roche lobe**.

A considerable mass outflow and oblique incidence of X-rays may result, for the

* If the observational data will allow to ascertain such occultations then the possibility (1) will fall away, for the disc existence most likely testifies the accretion to continue.

** Shklovsky, considering Sco X1 as the component of a binary system believes that a considerable massloss rate is a particular feature of the normal component – the dwarf, which does not fill its Roche lobe [45].

soft X-ray spectrum $kT_x \sim 5$ keV, in an absorption of the major part of the X-ray flux in the optically thin for the optical radiation region (Section 3.6.). The analysis of the numerical results for the models S (1) and S (10) shows that a rather small fraction $\beta_{opt} \lesssim 10\%$ of the X-ray flux may be re-radiated in the optical range. The optical flux towards the observer due to the X-ray reprocessing is given by (see Figure 11).

$$f_{opt} = f_x \beta_{opt} R^2 \int_{R/A}^{1} d\cos\vartheta \int_{-\pi/2}^{\pi/2} \frac{\sin\delta_1 \cos\psi \cos\delta}{l^2} d\varphi \approx$$

$$\approx f_x \beta_{opt} \frac{\pi}{8} \left(\frac{R}{A}\right)^3 \left(1 - \frac{R}{2A}\right), \tag{63}$$

where f_x[erg cm^{-2} s^{-1}] is the X-ray flux; and A is the separation of the components centres. The factor $(1 - R/2A)$ appears due to the dependence of the flux from the hot spot f_{opt} on the angle of observation Θ (for $i = 0$ the brightness of the spot is less than at the phase 0.5 for $i = 90°$, cf. Section 5.3.1.).

From equation (63) we can see that, due to the X-ray beaming ($\sin\delta_1 \propto R/A$), the ratio f_{opt}/f_x decreases proportionally to $(R/A)^3$ instead of $(R/A)^2$ with increasing A. Inserting $\beta_{opt} = 0.1$ and $f_{opt}/f_x = 10^{-4}$ we find the radius of the normal component $R = 0.14\,A$. For $\mathcal{M}_x/\mathcal{M}_v = \gamma > 1$ instead of (58) we have from [43].

$$R/A = \eta(\gamma) = 0.378\,\gamma^{-0.274}. \tag{64}$$

Now we readily obtain (cf. also [42]) $\gamma = \gamma_1 \approx 35$. It should be noted that this estimate is very sensitive to the ratio L_{opt}/L_x adopted. For $f_{opt}/f_x = 3 \times 10^{-4}$ and $\beta_{opt} = 0.1$ we find $\gamma = \gamma_2 = 10$ and for $f_{opt}/f_x = 10^{-3}$ and $\beta_{opt} = 0.1$ we even have $\gamma = \gamma_3 = 2$.

If Sco X1 is at a distance 1 kpc, its X-ray luminosity is equal to $L_x \approx 3 \times 10^{37}$ erg s^{-1}. The optical luminosity of the normal component can then approximate that of the Sun. Adopting its mass to be $\mathcal{M}_\odot$ and the radius $R = 10^{11}$ cm, we obtain the other parameters of the system $\mathcal{M}_x/\mathcal{M}_\odot = 2\text{–}10\text{–}35$ and $A = (3\text{–}5\text{–}7) \times 10^{11}$ cm corresponding to the values γ_3, γ_2 and γ_1.

It is worth noting that, for the dense and compact normal component, the calculations of the Roche lobe parameters [42], [43] may disagree with the real situation and the restrictions for $\gamma = \mathcal{M}_x/\mathcal{M}_v$ may turn out to be less severe. It is also important to obtain from the observations more precise restrictions for L_1 and L_2 which considerably influence the parameters of the system. The answer to the question whether Sco X1 is a binary system to a great extent depends on the results of simultaneous optical and X-ray variability observations, and on the results of the theory of stellar evolution in binary systems which may allow them to obtain the component masses possible.

As the binary nature of X-ray sources can be mainly ascertained for eclipsing systems ($i > 60°$), it is very likely that a considerable number of X-ray sources of the Sco X1-type are components of binary systems with $i < 60°$; and, being black holes, radiate by accretion.

Appendix

A. IONIZATION EQUILIBRIUM

As an X-ray photoabsorption cross-section per hydrogen atom, the power interpolation of the results from [29] for the gas with normal chemical abundances was used in the form

$$\sigma_{\mathrm{O}}(\nu) = 2.5 \times 10^{-22} (\nu_0/\nu)^{2.4} \text{ cm}^2, \quad \text{for} \quad h\nu > \chi_{\mathrm{O}} \tag{A1}$$

where $\nu_0 = 2.42 \times 10^{17}$ HZ is the frequency of a photon with the energy $h\nu_0 = 1$ keV, $\chi_{\mathrm{O}} = 870$ eV is the ionization potential of O VIII. For $h\nu < \chi_{\mathrm{O}}$ the photoabsorption was assumed to be due to the neutral helium [29]

$$\sigma_{\mathrm{He}}(\nu) = 0.73 \times 10^{-22} (\nu_0/\nu)^3 \text{ cm}^2 \tag{A2}$$

For $\nu > \nu_0$ the oxygen makes the main contribution to the photoabsorption cross-section [29], [30]. For this reason the ionization equilibrium was calculated between O IX and O VIII for oxygen, and between He II and He III for helium. Thus obtained abundances of He II and O VIII were assumed to be equal to a sum of the abundances of He I and He II for helium, and a sum over O VIII and lower ionization stages for oxygen. For O VIII and lower ionization stages of oxygen the photoabsorption cross section was calculated according to (A1) and for He I and He II – according to (A2).

The ionization equilibrium between O VIII and O IX was determined with respect to two processes: X-ray photoionization and recombination. For He II the electron impact ionization was taken into account. For the calculations of recombination rate coefficients, equations for hydrogen-like atoms were used [54] in the form

$$\alpha_{\mathrm{O}}(T) = 1.34 \times 10^{-9} T^{-1/2} \varphi(1.01 \times 10^7/T) \text{ cm}^3 \text{ s}^{-1}, \tag{A3}$$

$$\alpha_{\mathrm{He}}(T) = 0.836 \times 10^{-10} T^{-1/2} \varphi(6.32 \times 10^5/T) \text{ cm}^3 \text{ s}^{-1}, \tag{A4}$$

$$\varphi(x) = \sum_{n=1}^{\infty} x n^{-3} \int_0^{\infty} e^{-\xi} (\xi + x n^{-2})^{-1} \, \mathrm{d}\xi \approx \tfrac{1}{2} \left(1.735 + \ln x + \frac{1}{6x} \right). \tag{A5}$$

For the equilibrium fractional abundances of O VIII and He II we have

$$c_{\mathrm{O}}(T, \varrho, r) = \frac{\alpha_{\mathrm{O}}(T) \, x_e x_{\mathrm{O}} \varrho}{\alpha_{\mathrm{O}}(T) \, x_e x_{\mathrm{O}} \varrho + x_{\mathrm{H}} m_p \int_{\nu_e}^{\infty} [\mathscr{F}_x(\nu, r)/h\nu] \, \sigma_{\mathrm{O}}(\nu) \, \mathrm{d}\nu}, \tag{A6}$$

$$c_{\mathrm{He}}(T, \varrho, r) = \frac{\alpha_{\mathrm{He}}(T) \, x_e x_{\mathrm{He}} \varrho}{[\alpha_{\mathrm{He}}(T) + q_i(T)] \, x_e x_{\mathrm{He}} \varrho + x_{\mathrm{H}} m_p \int_{\nu_2}^{\infty} [\mathscr{F}_x(\nu, r)/h\nu] \, \sigma_{\mathrm{He}}(\nu) \, \mathrm{d}\nu}, \tag{A7}$$

where x_{O} and x_{He} are the numbers of oxygen and helium nuclei per nucleon, $q_i(T)$ is

the rate coefficient of He II electron impact ionization. The latter was calculated from the approximate expression from [55], of the form

$$q_i(T) = 3.54 \times 10^{-11}\, T^{0.345} \exp(-6.32 \times 10^5/T)\ \mathrm{cm}^3\ \mathrm{s}^{-1}. \tag{A8}$$

The electron number per nucleon x_e was calculated according to the Saha's formula

$$x_e = x_{\mathrm{H}}(\sqrt{1+4\xi} - 1)/2\xi, \tag{A9}$$

where $\xi = 2.5 \times 10^8\, \varrho T^{-3/2} \exp(1.58 \times 10^5/T)$.

B. THE ENERGY LOSS RATE AND OPTICAL DEPTH

For the free-free emission we have [56]

$$\varkappa_{ff}(\nu, T, \varrho) = 3.7 \times 10^8\, N_e(\sum_i N_i Z_i^2)\, T^{-1/2}\nu^{-3}[1 - \exp(-h\nu/kT)]\ \mathrm{cm}^{-1}, \tag{A10}$$

where N_e and N_i are the numbers of electrons and ions of charge Z_i per unit volume. The Gaunt factor is equal to unity. Inserting (A 10) into (6) and performing the integration we find

$$q_{ff}^-(T, \varrho) = 5.2 \times 10^{20}\, \varrho x_e(\sum_i x_i Z_i^2)\, T^{1/2}(1 - [(T_{\mathrm{eff}}/T)\, \Phi(T_{\mathrm{eff}}/T)]\ \mathrm{erg}\, g^{-1}\, \mathrm{s}^{-1}, \tag{A11}$$

where $\Phi(x) = \int_0^1 (1-\xi^x)(1-\xi)^{-1}\, \mathrm{d}\xi$. The most interesting for us is the behaviour of $\Phi(x)$ near unity, where it can be approximated by $\Phi(x) \approx x^{0.645}$. For the photoabsorption cross-section of negative hydrogen ions the approximate formula

$$\sigma_H(\nu) = 6.4 \times 10^{-16}[2(\nu/\nu^*) - 1]\, \{(\nu/\nu^*)^2\, [(\nu/\nu^*)^2 + 16]\}^{-1}\ \mathrm{cm}^2 \tag{A12}$$

was used for $\nu \geqslant \nu^*/2$, where $\nu^* = 3.63 \times 10^{14}$ HZ. This expression offers a reasonable approximation to more accurate calculations by various authors [57]. Using the Saha's formula for determination of the number of negative hydrogen ions and (A12) we obtain

$$\varkappa_{\mathrm{H}}(\nu, T, \varrho) = 4.3 \times 10^{-33}\, N_e N_{\mathrm{H\,I}} T^{-3/2} \exp(8.7 \times 10^3/T)\, [2(\nu/\nu^*) - 1] \times \\ \times (\nu^*/\nu)^2\, [1 + (\nu/\nu^*)^2/16]^{-1}\, [1 - \exp(-h\nu/kT)]\ \mathrm{cm}^{-1}. \tag{A13}$$

The absorption coefficient for the photoionization of nth hydrogen atom level (for the Boltzmann level population) is given by [56]

$$\varkappa_{rn}(\nu, T, \varrho) = 1.15 \times 10^{14}\, N_e^2 T^{-3/2} n^{-3} \nu^{-3} \times \\ \times \exp(\chi_n/kT)\, [1 - \exp(-h\nu/kT)]\ \mathrm{cm}^{-1} \tag{A14}$$

for $h\nu \geqslant \chi_n$. Under these conditions we may assume that $(\nu/\nu^*) \ll 4$, $\exp(\chi_n/kT) \gg 1$, $\exp(h\nu^*/2kT) \gg 1$; then we have

$$q_H^-(T, \varrho) = 1.67 \times 10^{19}\, \varrho x_e x_{\mathrm{H\,I}} T^{1/2}(1 + 2.22 \times 10^{-4}\, T) \times \\ \times \{1 - (T_{\mathrm{eff}}/T)^2\, [4kT_{\mathrm{eff}}/h\nu^* + 1] \exp(h\nu^*/2kT - \\ - h\nu^*/2kT_{\mathrm{eff}})\, [4kT/h\nu^* + 1]^{-1}\}\ \mathrm{erg/g.\,s}. \tag{A15}$$

and

$$q_{rn}^{-}(T, \varrho) = 1.6 \times 10^{26}\, \varrho x_e^2 T^{-1/2} n^{-3} \times \\ \times [1 - (T_{\text{eff}}/T) \exp(\chi_n/kT - \chi_n/kT_{\text{eff}})] \text{ erg } g^{-1}\, s^{-1}. \quad \text{(A16)}$$

The optical depth at every point r was calculated according to

$$\tau(\nu, r) = \int_r^{\infty} [\varkappa_{ff}(\nu, T, \varrho) + \varkappa_H(\nu, T, \varrho) + \sum_{n=2}^{\infty} \varkappa_{rn}(\nu, T, \varrho)]\, dr. \quad \text{(A17)}$$

Acknowledgements

The authors greatly appreciate the useful discussions with Ya. B. Zeldovich and N. I. Shakura. We wish to thank L. R. Yangurazova for assistance and L. A. Teutchezh for preparation of the paper. We have also benefited from the conversations with G. S. Bisnovaty-Kogan, A. M. Cherepashchuk, Yu. N. Efremov, V. S. Imshennik, B. V. Komberg, N. E. Kurochkin and I. S. Shklovsky.

References

[1] H. Tananbaum: 1973, in H. Bradt and R. Giacconi (eds.), 'X- and Gamma-Ray Astronomy', *IAU Symp.* **55**, 9.
[2] M. Gursky: 1972, Preprint 'Galactic X-Ray Sources', Lectures in Les Houches.
[3] I. S. Shklovsky: 1967, *Soviet Astron.* **44**, 930.
[3a] O. H. Huseynov: 1970, *Soviet Astron.* **47**, 1143.
[4] N. I. Shakura and R. A. Sunyaev: 1972 Preprint of Inst. Appl. Math., No. 28, Moscow; 1973, *Astron. Astrophys.* **24**, 337.
[5] H. Tananbaum, H. Gursky, E. M. Kellogg, R. Levinson, E. Schreier and R. Giacconi: 1972, *Astrophys. J.* **174**, L143.
[6] W. Liller: 1972, *IAU Circ.*, No. 2415.
[7] N. E. Kurochkin, 1972, *Astron. Circ.* No. 717.
[8] K. Brecher: 1972, *Nature* **239**, 325.
[9] A. M. Cherepashchuk, Yu. N. Efremov, N. E. Kurochkin, N. I. Shakura, and R. A. Sunyaev: 1972, *Inform. Bull. Var. Stars* No. 720.
[10] V. M. Lyutiy, R. A. Sunyaev, and A. M. Cherepashchuk: 1972, Preprint of Inst. Appl. Math. **61**, Moscow; 1973, *Soviet Astron.* **50**, 3.
[11] J. N. Bahcall and N. A. Bahcall: 1972, *Astrophys. J.* **178**, L1.
[12] W. Forman, C. A. Jones, and W. Liller: 1972, *Astrophys. J.* **177**, L103.
[13] D. Ya. Martynov: 1971, in *Eclipsing Variable Stars,* Moscow, p. 155.
[14] M. M. Basko, Yu. N. Efremov, R. A. Sunyaev, and A. M. Cherepashchuk; 1973, *Soviet Astron.* (in press).
[15] B. V. Kukarkin, P. P. Parenago, Yu. N. Efremov, and P. N. Cholopov: 1969–1971, *The General Catalogue of Variable Stars,* 3rd ed., 1–3, Moscow.
[16] M. P. Ulmer, W. A. Baity, W. A. Wheaton, and L. E. Peterson: 1972, *Astrophys. J.* **178**, L61.
[17] D. Crampton and J. B. Hutchings: 1972, *Astrophys. J.* **178**, L65.
[18] B. W. Bopp, G. Grupsmith, and P. Van den Bout: 1972, *Astrophys. J.* **178**, L5.
[19] I. D. Novikov and Ya. B. Zeldovich: 1966, *Nuovo Cimento Suppl.* **4**, 810.
[20] K. H. Prendergast and G. R. Burbidge: 1968, *Astrophys. J.* **151**, L83.
[21] N. I. Shakura: 1972, *Soviet. Astron.* **49**, 921.
[22] J. P. Pringle and M. J. Rees: 1972, *Astron. Astrophys.* **21**, 1.
[23] I. D. Novikov and K. S. Thorne: 1972, Preprint, 'Astrophysics of Black Holes', Lectures in Les Houches.

[24] J. Ostriker and R. Davidson: 1973, in H. Bradt and R. Giacconi (eds.), 'X- and Gamma-Ray Astronomy', *IAU Symp.* **55**, 143.
[25] N. E. Kurochkin: 1973, *Inform. Bull. Var. Stars* No. 55.
[25a] M. M. Basko, R. A. Sunyaev, and L. G. Titarchuk: 1973, Preprint of Institute of Space Research; *Astron. Astrophys.* (in press).
[26] N. I. Shakura and R. A. Sunyaev: 1973, in H. Bradt and R. Giacconi (eds.), 'X- and Gamma-Ray Astronomy', *IAU Symp.* **55**, 143.
[27] T. E. Holzer and W. I. Axford: 1970, *Ann. Rev. Astron. Astrophys.* **8**, 31.
[28] V. V. Sobolev: 1967, *The Course of Theoretical Astrophysics,* Moscow.
[29] K. L. Bell and A. E. Kingston: 1967, *Monthly Notices Roy. Astron. Soc.* **136**, 241.
[30] R. L. Brown and R. J. Gould: 1970, *Phys. Rev. D.* **1**, 2252.
[31] H. Frish: 1972, *Space. Sci. Rev.* **13**, 455.
[32] C. B. Tarter, W. H. Tucker, and E. E. Salpeter: 1969, *Astrophys. J.* **156**, 943.
[33] E. V. Levich and R. A. Sunyaev: 1971, *Soviet Astron.* **48**, 461.
[34] G. B. Field: 1970, in H. J. Habing (ed.), 'Interstellar Gas Dynamics', *IAU Symp.* **39**, 51.
[35] S. B. Pikelner: 1967, *Soviet. Astron.* **44**, 1915.
[36] Ya. B. Zeldovich and R. A. Sunyaev: 1969, *JETP* **56**, 2078.
[37] B. Paczynski: 1971, *Ann. Rev. Astron. Astrophys.* **9**, 183.
[38] S. Kříž: 1970, *Bull. Astron. Inst. Czech.* **21**, 211.
[39] V. G. Gorbatzky: 1967, *Astrophysics* **3**, 245.
[39a] P. R. Amnuel and O. H. Huseynov: 1972, *Astrophysics* **8**, 107.
[40] Yu. N. Gnedin and R. A. Sunyaev: 1973, *Astron. Astrophys.* (in press).
[41] A. Davidsen, J. P. Henry, J. Middleditch, and M. E. Smith: 1972, *Astrophys. J.* **177**, L97.
[42] Z. Kopal: 1959, *Close Binary Systems,* Wiley, New York.
[43] M. Plavec and P. Kratochvíl: 1964, *Bull. Astron. Inst. Czech.* **15**, 165.
[44] W. Wenzel and M. Hessner: 1972, *IBVS* **733**; *Mitteil. Veränder. Stern.* (in press).
[45] I. S. Shklovsky: 1973, *Soviet. Astron. J.* **50**, 233.
[46] H. A. Bethe and E. E. Salpeter: 1957, *Quantum Mechanics of One- and Two-Electron Atoms,* Acad. Press, New York.
[47] G. W. Clark, H. V. Bradt, W. H. G. Lewin, T. H. Markert, H. W. Schnopper, and G. F. Sprott: 1972, *Astrophys. J.* **177**, L109.
[48] V. V. Ivanov: 1969, *Radiative Transfer and Celestial Body Spectra,* Moscow.
[49] F. K. Lamb, C. J., Pethick, and D. Pines: 1972, Preprint: *Astrophys. J.* (in press).
[50] B. V. Komberg: 1973, Preprint of Inst. Appl. Math.
[51] I. D. Novikov: 1973, *Soviet. Astron.* J. (in press).
[52] S. A. Zhevakin: 1963, *Ann. Rev. Astron. Astrophys.* **1**, 367.
[53] G. Neugebauer, J. B. Oke, E. Becklin, and G. Garmire: 1969, *Astrophys. J.* **155**, 1.
[54] G. R. Burbidge, R. J. Gould, and S. R. Pottasch: 1963, *Astrophys. J.* **138**, 945.
[55] A. G. Doroshkevich and R. A. Sunyaev: 1967, Preprint of Inst. Appl. Math.
[56] S. A. Kaplan and S. B. Pikelner: 1963, *Insterstellar Medium,* Moscow.
[57] L. Branscombe: 1962, in D. R. Bates (ed.), *Atomic and Molecular Processes,* Acad. Press, New York and London.